Acta Crystallographica Section A
Foundations of Crystallography
ISSN 0108-7673

Received 16 October 2009
Accepted 14 December 2009

'Making the molecular movie': first frames

R. J. Dwayne Miller,[a]* Ralph Ernstorfer,[a,b] Maher Harb,[a,c] Meng Gao,[a] Christoph T. Hebeisen,[a,d] Hubert Jean-Ruel,[a] Cheng Lu,[a] Gustavo Moriena[a] and German Sciaini[a]

[a]Departments of Chemistry and Physics, and Institute for Optical Sciences, University of Toronto, 80 St George Street, Toronto, Ontario, Canada M5S 3H6, [b]Physik Department E11, Technische Universität München, D-85747 Garching, Germany, [c]Department of Atomic Physics, Lund University, PO Box 118, SE-221 00 Lund, Sweden, and [d]Joint Laboratory for Attosecond Science, University of Ottawa and National Research Council, 100 Sussex Drive, Ottawa, Ontario, Canada K1A 0R6. Correspondence e-mail: dmiller@lphys.chem.utoronto.ca

Recent advances in high-intensity electron and X-ray pulsed sources now make it possible to directly observe atomic motions as they occur in barrier-crossing processes. These rare events require the structural dynamics to be triggered by femtosecond excitation pulses that prepare the system above the barrier or access new potential energy surfaces that drive the structural changes. In general, the sampling process modifies the system such that the structural probes should ideally have sufficient intensity to fully resolve structures near the single-shot limit for a given time point. New developments in both source intensity and temporal characterization of the pulsed sampling mode have made it possible to make so-called 'molecular movies', *i.e.* measure relative atomic motions faster than collisions can blur information on correlations. Strongly driven phase transitions from thermally propagated melting to optically modified potential energy surfaces leading to ballistic phase transitions and bond stiffening are given as examples of the new insights that can be gained from an atomic level perspective of structural dynamics. The most important impact will likely be made in the fields of chemistry and biology where the central unifying concept of the transition state will come under direct observation and enable a reduction of high-dimensional complex reaction surfaces to the key reactive modes, as long mastered by Mother Nature.

1. Introduction

1.1. 'Molecular movies': spatial–temporal intensity-source requirements

One of the great scientific challenges of our times is to directly observe atoms during the primary processes governing physical phenomena (King *et al.*, 2005; Dwyer *et al.*, 2006). The concept of the atomic structure of matter was established well over a century ago and is now part of our collective consciousness. With the development of field ion microscopes, electron microscopes and scanning probe microscopes we can even directly observe atoms in real space. However, static pictures of matter do not tell us how things happen. The world is dynamic.

Biologists routinely discuss how ligands bind at active sites, how DNA unwinds, or how protein regulation occurs. These concepts typically involve picturing how atoms move relative to one another in the process. Similarly, chemists are trained to discuss atomic motions during chemical processes. Physicists likewise treat phenomena such as phonons, phase transitions *etc.* in terms of collective coordinates involving an atomic basis. These different points of view from different disciplines have one feature in common: they involve discussions of dynamical phenomena within an atomic basis. It is well recognized that finer levels of inspection uncover new details and bring a higher level of understanding. For this reason, there is an inherent desire to directly observe atoms move during dynamical processes. This objective represents the spatial–temporal limit to observations of the primary events defining chemistry and biology.

Until recently, the direct observation of atomic motions in real time during structural transitions has been considered the exclusive domain of thought experiments, outside the realm of direct experimental observation. This position can be readily appreciated by considering the challenge of making a molecular movie camera to capture such motions. The first consideration is the required shutter speed. Take, for example, the most basic chemical event of bond breaking. What would the shutter speed need to be, *i.e.* what is the timescale involved in breaking chemical bonds? First, we have to define when a chemical bond is broken. Take a typical interatomic potential as a starting point. If two masses are separated by approximately twice the equilibrium bond length, the potential is no longer attractive within kT (ambient conditions). At this

point, the bond can be considered broken. For thermally sampled coordinates, the fastest two atoms could move along a bond-breaking coordinate would be at the speed of sound. To keep things simple, assume an equilibrium bond length of 1 Å and a speed of sound typical for organic materials, of approximately 10^5 cm s^{-1}, then the time it would take the bond to break is the time it takes the two masses to move 1 Å along the bond dissociation coordinate at the speed of sound or 100 fs. More rigorous analysis can be done using transition-state theory to discuss the displacements of the most anharmonic modes that contribute most to the reaction energetics. These modes are always typically in the 10–100 cm^{-1} range, again giving approximate timescales of 100 fs for the sampling period (Miller, 2002; Polanyi & Zewail, 1995). Also, typical prefactors in the Arrhenius expression for unimolecular rate constants are approximately 10^{13} s^{-1}, once again 100 fs sampling frequencies of the reaction coordinate. To be sure, there are faster atomic motions. For example, the OH stretch vibration of water molecules has a period of 10 fs. However, the r.m.s. motion is on the order of 0.05 Å not the 1 Å scale needed for irreversible structural changes. There are faster and slower timescales for different reactions but this 100 fs window serves as the canonical shutter speed required for making so-called 'molecular movies'.

The relevant timescale has been known since Arrhenius' time. This timescale of one ten millionth of a millionth of a second would have seemed unapproachable up to 25 years ago. However, with modern laser technology we now push the boundaries of monitoring molecular dynamics down to the attosecond (10^{-18} s) timescale (Corkum & Chang, 2008). Femtosecond laser systems are commercially available with time resolution superior to the required effective shutter speed of 100 fs. It is not the time resolution that remains elusive. As all good directors know, in order to make a great movie, one must catch the actors with the correct lighting. In our movie, the 'actors' are the atoms. In order to spatially resolve the atomic positions one requires the use of a source of lighting with wavelengths on the atomic length scale, *i.e.* one must use either hard X-rays in the 10 keV range or alternatively electrons with de Broglie wavelengths of 1 Å or less. The real challenge from an experimental point of view is to develop a source with enough X-ray photons or electrons to light up the atomic motions in a single frame or time snapshot. This statement is made as the process of directly observing atomic motions requires a perturbation or excitation step that synchronizes the event of interest. Generally speaking, the experiments require excitation levels sufficient to excite 1–10% of the atoms/molecules involved in order to clearly resolve the dynamics above the background. The excitation process, not the monitoring process, makes the process generally irreversible. The system typically does not return exactly back to the starting conditions. Thus, one must come up with a lighting source that is sufficiently bright to obtain full structures at atomic resolution in a single shot. If not, the amount of sample required for irreversible processes quickly becomes intractable. This statement is made as a generalization of sample conditions. There are a precious few samples that can be excited repeatedly, as will be discussed, and then low brightness sources can be used. In all cases, however, one would like as bright a source as possible and still retain the required spatial and temporal resolution to observe atomic motions.

The real challenge undertaken by our group was to make a 'molecular movie camera' with enough flux to essentially capture structures at the atomic level in a single shot – using electrons. For practical reasons, we need to work with tabletop systems and the prospect of a tabletop X-ray source with sufficient brightness is many decades in the future yet. Now consider the fundamental problem of using electrons. We needed to have enough electrons in a pulse of subpicosecond duration and cross-sectional area to approach single-shot structure determination without using up huge amounts of material for the 'molecular movie film'. Here it is important to realize that the sample thickness has to be on the order of 10–100 nm, depending on the electron energy, so that the electron diffraction process to monitor atomic motions occurs in the single-electron scatter limit for simple inversion of the diffraction pattern. It is extremely difficult to make free-standing samples this thin with the required crystallinity, flatness and sufficient surface area. It is essential to be as economical as possible in the number of laser shots per time point taken to capture a molecular movie. The number of electrons has to be sufficient to get as close to single-shot structure determinations as possible. Here it is important to recall that electrons are charged particles that undergo electron–electron repulsion and will be hard to coerce into a very short pulse. The natural tendency is for electron–electron repulsion, or space-charge effects, to lead to pulse broadening. At the time we started this research, it was thought to be impossible to have sufficient electron densities to approach single-shot structure determinations. We have achieved this requirement as will be discussed below through a detailed investigation of the fundamental limits in electron-source brightness.

Fig. 1 shows a picture of the 'fourth-generation electron gun' currently used by our group as well as a picture of a typical diffraction pattern captured using fs electron pulses.

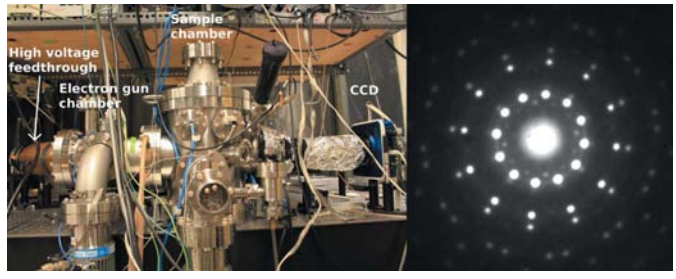

Figure 1
Left panel: sample chamber and the electron gun. Right panel: diffraction pattern of (111)-oriented Bi. A more detailed experimental layout is given in Fig. 2.

1.2. Operational definition of 'molecular movies'

The term 'molecular movie' has been used in a number of different contexts. Here we argue for a specific definition. Movies allow motions to be recorded so that the causal events of interest can be fully observed. In a number of applications, the term 'molecular movie' has been used to describe the determination of transient structures on the 100 ps to μs and even longer timescales (Srajer *et al.*, 2001; Schotte *et al.*, 2003). These structures are extremely valuable for determining intermediates and reducing the number of 'possible pathways' connecting structures (Coppens, 2003) but they do not enable an unambiguous determination of the actual mechanism or specific pathway. The structural information collected in this way is akin to time-lapse photography. The details connecting changes are missing. As a crude analogy, before and after photos of someone undergoing weight loss does not tell how the weight was lost or what regime of diet and exercise was used. It is not possible to determine how the change occurred if the structural changes are not followed on the relevant timescales for mechanistic details. *At the atomic level, to qualify as a 'molecular movie', the time and space resolution must be sufficient to follow the atomic motions faster than collisions lead to diffusive motions that wash out or blur the force correlations between atoms that lead to the change in structure*. If not, one has a 'before' laser excitation and 'after' laser excitation structure with no clear pathway connecting the two structures. The information on transient intermediates is important in its own right but does not provide sufficient mechanistic information. One is left to models to fill in the details. To follow the key motions leading from one structure to another requires nominally sub-ps time resolution to atomic motions as discussed above. The same holds true for gas-phase reaction dynamics where there are no collisions. In this case, the structural dynamics need to be recorded faster than the periods of the reactive modes.

1.3. The big (motion) picture

1.3.1. Direct observation of transition states. One of the most important concepts in chemistry is the notion of a transition state. This concept describes the intersection between a reactant and product surface along a reaction coordinate. The idea that there is a singularity in this surface at which point small fluctuations take the system from nuclear configurations defining the reactant to those of the product state dates back to 1935 (Evans & Polanyi, 1935; Eyring, 1935). There are fairly detailed microscopic models of such processes in which specific structures are proposed for motion along the reaction coordinate. There is a strong desire to connect reaction pathways to structural changes as this gives some insight into how to control barriers and thereby chemical reactions.

The transition state is structurally depicted as the halfway point along the displacement of some principal reaction mode. For example, in the case of *trans*- to *cis*-isomerization, the reaction mode is the torsion or rotational motion around a double bond. The transition state is defined to be at the 90° point in the rotation about this bond (Seidner & Domcke, 1994; Abe *et al.*, 2005). Even in the simplest case, there is also a coupling mode such as the stretching or softening of the double bond in the above example. Reaction coordinates need to be depicted by multidimensional surfaces. In principle, all the atomic motions of the reactants are coupled and affect the reaction forces leading to product formation. For small molecular systems, say ten atoms or less, there are generally well defined reaction modes so the dimensionality of the problem, as in the case of isomerization, can be reduced to a manageable level. For such systems, we have very good descriptions of transition states and pictures of nuclear passage through the transition-state region. However, the complexity of the problem quickly scales with the number of atoms involved and the dimensionality does not lend itself well to even highly simplified potential energy surfaces. Reactions occurring in solution phase or within proteins are just a few examples where simple pictures need to be challenged (Voth & Hochstrasser, 1996; Adelman, 1987). There are not unique pathways connecting the reactant surface to the product surface. There are numerous, even innumerable, pathways through the transition-state region. In this case, the reaction coordinate is better represented as a free energy surface for which the different barrier-crossing configurations are lumped into the entropic terms of the free energy surface. Even with this representation, there is still a strong motivation to connect the free energy surface to a narrow distribution of structures.

Here, we can further reflect on the importance of determining the potential energy surface for a chemical reaction. Significant efforts have been expended in the chemical physics community using molecular beam methods in combination with spectroscopy and theory to derive such surfaces (Polanyi & Zewail, 1995). For small molecular systems, where this is possible, there is an enormous amount of information in such diagrams (Pilling & Seakins, 1995). It is possible, for any given nuclear configuration, to visualize the potential energy gradients or forces on the atoms, pushing them along the reaction coordinate. We can get a nearly visceral feel for the reaction and how it occurs. However, as discussed, this depiction is not possible for molecules beyond a few atoms. In contrast, if we could directly visualize atomic motions during a chemical reaction, we would have the same fundamental information of interest as embedded in the most rigorous potential energy surfaces for small-molecule reactions. We would have the mass- and time-dependent velocities (forces) for even the most complex molecular systems. Most importantly, the entire multidimensional reaction coordinate would be reduced to the principal modes involved in directing the process and would thereby define the barrier region.

The recent development of ultrabright electron, and soon hard X-ray, sources to directly observe atomic motions on the fs timescale is opening up the exploration of reaction dynamics of complex molecules and providing the same level of rigor previously only obtainable for small-molecule systems using a multitude of different experimental and theoretical methods. This information content is obtained in a single measurement. Equally important, it is difficult to extend

concepts from studies of small, well defined molecules in the gas phase, for example, to solution-phase chemistry or heterogeneous chemistry that define the majority of the chemical processes of interest (Adelman, 1987). This experimental methodology will have a significant impact in terms of providing a truly atomic level understanding of actual chemical reactions used in practice.

1.3.2. Quest for the structure–function correlation in biology. One of the central tenets of biology is that biomolecules have optimally evolved to direct chemistry by control over barriers or the transition state (Nagy *et al.*, 2006). Mother Nature is the grand master of controlling chemical processes to do work on the surroundings as part of a biological function.

Chemical reactions power biological functions and the various structures of the biomolecules are highly evolved to act as heterogeneous catalysts for the particular functional response. If we consider a simple ligand dissociation process, the initial event of bond breaking clearly occurs over atomic length scales and is quantum mechanical in nature. However, this relatively minute amount of energy must couple to some thousands of other atomic degrees of freedom to execute a biological function over mesoscale dimensions. Herein lies the wonder of biological processes. The bond-breaking event is clearly quantum mechanical in nature and involves fluctuations on the Å length scale. The quantum singularity of bond breaking must propagate out to the nm or mesoscale and couple to thousands of atoms to perform a biological function, *i.e.* to do work on the surroundings. The number of degrees of freedom coupled to the single act of a bond-breaking process or other chemical reaction is enormous. The amount of energy distributed over these degrees of freedom is marginally larger than the background thermal energy yet these processes work nearly unerringly. Mother Nature clearly understands quantum mechanics and the correspondence principle in optimally channelling chemical energy into biological functions – coupling quantum systems to the classical mechanics continuum limit.

How do we understand this energy transduction process? Here, a concrete example helps depict the key concepts at stake. The simple act of oxygen binding to hemoglobin serves as one of our best understood systems. In the process of oxygen transport in the body, somewhere between the dissociation of two to three oxygen molecules, hemoglobin undergoes a remarkable 15° rotation between the α and β protein subunits and a 6 Å translation in a type of ball-and-socket motion about the quaternary contacts, involving some 10 000 degrees of freedom. This change in quaternary structure causes a change in binding efficacy of nearly a factor of 100 for diatomic oxygen through structural modification of the barriers to ligand binding. Based on static structures, obtained with and without a ligand bound to the iron, we have developed a fairly detailed picture of the sequence of events leading to molecular cooperativity in the binding of oxygen. In this context, hemoglobin serves as our cornerstone in the understanding of molecular cooperativity in general (Perutz *et al.*, 1976). But is the picture correct?

In myoglobin the breaking of the bond leads to homolytic cleavage with an electron becoming localized on the *d* orbitial of the iron. The iron effectively becomes bigger, experiences repulsive forces that force it out of plane (doming) and pushes against the proximal histidine. A series of cascaded events localized at the proximal histidine are envisaged, akin to a series of falling dominoes, the size of single amino acids, that lead to the overall motion of the EF helix. It is this motion of the helical sections that ultimately leads to changes in the contact forces of hemoglobin and drives the quaternary structure changes. Effectively, it is the coupling of the heme doming to the helical motions that affects the barrier height for ligand binding. Changes in structure alter the force needed for motion along the doming coordinate and thereby give a through-space coupling of reaction coordinates to affect molecular cooperativity, the simplest form of molecular feedback and signaling. It is important to note that the above description inherently assumes a localized correlation length scale for the primary motions of the reaction, *i.e.* a localized basis. This distinction is important as site-directed mutagenesis for modification of protein functions is based on a localized picture of the reaction coordinate.

If one examines this model for the motions based on static X-ray structures, it would appear that the key motions are all along the normal to the heme ring. If so, it is a simple matter to provide a structural basis for the transition state and think about means to control the barrier height. The transition state would simply be the iron motion out of plane to a position halfway between the fully domed configuration and all motions would be along the heme normal. By photodissociating the Fe—CO bond of carboxymyoglobin with few cycle, 6 fs, pulses, we were able to determine that the bond dissociation occurs within 26 fs along a repulsive surface (Armstrong *et al.*, 2003). This motion is comparable to a half cycle of the Fe—CO stretch coordinate and is fast enough to impulsively excite all the reaction modes coupled to ligand dissociation in this far from equilibrium, optically accessed configuration. It turns out that, in order for the bond to break and heme to dome, the in-plane motions of the heme are also involved. The heavy atoms in the ring have to move to accommodate the Fe doming motion. These porphyrin ring modes are in turn coupled to the low-frequency helical motions through a series of cascaded motions over different length scales that are subharmonics of one another. The correlation length scale of the key reaction modes is global not local (Goodno & Miller, 1999; see figures in Miller, 2002). This single example shows the difficulty in connecting static structures to transition-state pathways.

The problem is further complicated by the enormous number of degrees of freedom in typical biological problems. If the protein were to function through a statical sampling of all possible degrees of freedom, it would take eons for a protein to perform its function. Clearly, proteins do not sample all possible nuclear configurations but rather coarse-grain sample through strongly correlated motions over different length scales. The correlations must be imposed by the distribution of structures within the protein's free energy

landscape. The problem is how do we connect the active structure of a protein to its function. If you are given a particular protein structure, can you tell how the protein works? This is the fundamental connection we need to make to understand how protein structures have evolved to optimally control chemical processes to perform their functions. The problem, however, must be reduced in complexity. We need to determine what is effectively a periodic table for structural biology in which specific topological features lead to a particular property with respect to directing chemical energy. Rudimentary examination of various protein structures suggests the number of identifiable topological units can be reduced to correlated motions of helices, beta sheets, loops and interconnection of topological units through tertiary contacts. How can we connect these topological features to the reaction coordinates driving biological function? Making this connection will give us the most fundamental understanding possible for biology.

To further get across the marvel of biochemical processes, consider the following analogy. Imagine you are attending a magnificent symphony for which some 10 000 different musicians have been assembled and who are all warming up their instruments as you enter a massive concert theatre. The sounds you would hear would be quite chaotic. Then the maestro steps forward, taps his baton and this marvellous music, the music of life (to overextend the metaphor), bursts forward. What just happened? The different degrees of freedom, the musicians, all agreed to be correlated through space by visual inspection of the conductor's baton. The scaling of this analogy is nearly correct. The motion and energy expended by the conductor is similar to that of the other musicians yet the conductor is able to correlate some 10 000 degrees of freedom. At the molecular level, the energy released with bond breaking is a small fraction of the total thermal energy of the protein and the r.m.s. motions are not similar for all degrees of freedom. In order for the relatively small amount of energy to orchestrate biological functions, there must be correlations imposed by the three-dimensional structure of the protein. In other words, to understand this problem, we are looking for the conductor's baton nestled within the various topological features of the protein's structure. In effect, biological molecules are examples of strongly correlated atoms. There is some incredible physics occurring to lead to such strong correlations and enormous speed up in reaction rates as occurs in Nature. We are effectively looking for the 'director' within the structural elements.

Based on experimental observation of global protein motions involved in the above problem of ligand dissociation in heme proteins, we proposed the collective mode coupling model as the mechanism for how proteins coarse-grain sample their potential energy surface (Miller, 2002). The 'director' in this model is the highly correlated secondary helical structures (and connected tertiary contacts) in relation to loops. This idea was also put forward by Seno & Go (1990) based on molecular dynamics (MD) calculations and modal analysis of the displacements. We showed that the global motions of heme proteins following ligand dissociation occurred on the same timescale as motions local to the bond dissociation coordinate. The different length scales of motion were 1:1 correlated. The correlation in motion over different length scales is the definition of a collective response. Furthermore, we developed new methods for measuring reaction energetics that showed this collective or inertial relaxation phase was the dominant component of the structural relaxation, *i.e.* the deterministic process (Miller, 2002; Walther *et al.*, 2005). The aforementioned work was able to observe more specifically the cascaded length scales of motion. In terms of the bond-breaking event of heme proteins, the doming of the heme is coupled to in-plane motions and further changes in contact points within the heme pocket that create a force displacing the helices surrounding the heme. It is a collective coordinate rather than a local coordinate as previously envisaged.

If one thinks of this mechanically, proteins are effectively hybrid states of matter, with solid-like and fluid-like compositional elements. The helical sections are rigid structural elements relative to the large r.m.s. motions of the loop regions. The motion of these sections leads to the atom–atom correlations.

Reaction coordinates are coupled to all possible degrees of freedom in the molecule–bath (surroundings) reference frame. The coupling coefficient is stronger for some types of thermally sampled degrees of freedom than others. For solution-phase chemistry, there appears to be no evidence for strong propensities; reactions seem to be dictated by density of states and damping terms. However, one would expect mode-selective coupling in biological systems. The structures of biological molecules surrounding reaction sites are highly anisotropic in contrast to the homogeneous, isotropic nature of solvation shells surrounding reaction partners in solution. We have indeed found this to be the case. The largest coupling coefficients, accounting for up to 80% of the structural relaxation/reorganization energetics along a reaction coordinate, are associated with a discrete number of collective modes. There have also been a number of theoretical studies (Zhang *et al.*, 2009) and experiments that show the involvement of collective modes (Cammarata *et al.*, 2008; Leu *et al.*, 2009). However, we cannot tell from the present experiments which motions are involved. We have to resort to MD-based methods and various approximations to cast out the key modes coupled to the reaction coordinate. Furthermore, most biologists will resist this picture unless it can be shown that the atomic motions are indeed correlated and do in fact map onto easily defined topological features.

Here is the crux of the structure–function correlation problem in biology. The collective mode coupling mechanism provides a nice framework to visualize strongly correlated motions. However, what motions are involved? The system is so complex that we cannot infer this information from any form of spectroscopy. The density of states and dimensionality of the problem are too enormous for such renderings. However, if we could directly observe atomic motions during the barrier-crossing event along a reaction coordinate, we would, in a single measurement, be able to cast out the prin-

Table 1
Comparison of electrons and X-rays for applications in atomically resolved dynamics.

Electrons	X-rays
Strongly scattered	Weakly scattered
Tabletop experiment	Tabletop for plasma sources only. Synchrotron/X-FELs/large frame laser
Pumped volume better matches scattering length of electrons	Large penetration depth, better suited for bulk studies
Multidiffraction orders facilitate structure determinations	Potential for Laue diffraction (not in the case of X-FELs)
Pulse duration dependent on electron number (DC electron gun)/recompression to <100 fs with single-shot structure capabilities and perfect synchronization of optical pump and electron probe	Pulse duration independent of photon number/estimate of 100 fs time resolution limited by timing jitter
Energy deposited in sample per scattering event 400–1000 times less (1.5 Å X-rays). Electron-induced sample damage is negligible	X-ray-induced damage limits crystal lifetime/diffract and destroy
Incoherent (for >1 μm beam diameters)	Coherent (X-FELs only)

cipal motions, *i.e.* we would have a direct observation of the structure–function correlation.

2. Technology developments

The emphasis of this review is on the development of high-number-density ('brightness') electron sources for real-time structural studies. There is a parallel effort ongoing in the development of X-ray sources, both tabletop laser-driven X-ray plasma source and next-generation light sources.

Table 1 shows that electrons interact much more strongly with matter than X-ray photons (Dwyer *et al.*, 2006). For the same energy, electrons scatter 10^6 times more strongly than X-rays. This difference means a factor of 10^6 fewer electrons are needed to give the same resolving power and signal-to-noise ratio (SNR) for the same energy electrons and X-rays for a given sample pathlength. The challenge as stated above is how to develop high-bunch-number electron pulses without Coulomb repulsion or space-charge degrading the spatial–temporal resolution. We have developed some relatively very 'bright' sources for this application. For comparison, a third-generation synchrotron, such as the ESRF in Grenoble, can produce quasimonochromatic, subnanosecond pulses consisting of 10^9 X-ray photons (Kim *et al.*, 2009). We have been able to achieve a few thousand electrons per pulse in a 200 fs pulse. Taking into account the much higher diffraction efficiency with electrons, the diffracted particle flux per sample pathlength (experimental figure of merit) is approximately 1000 times higher than a third-generation synchrotron. Only the fourth-generation X-ray free electron lasers (X-FELs) will be brighter when they come online with hard X-rays (http://www-ssrl.slac.stanford.edu/lcls/ or http://xfel.desy.de/). As will be discussed below, this difference in experimental brightness with respect to diffracted particle flux will soon be reduced with next-generation electron guns.

There are trade-offs, depending on the application, in which one source may be better than the other in extracting structural dynamics. For example, the larger penetration depth of X-ray sources makes them better suited to studies of solution-phase systems (Kim *et al.*, 2009); whereas in gas-phase studies the larger scattering cross section of electrons makes electrons the preferred source (Williamson *et al.*, 1992; Dudek & Weber, 2001). The one property of the new X-ray sources that would seem to be insurpassable is the coherence of the fourth-generation light sources. These are spatially coherent laser sources. The prospect of doing single-molecule reconstruction has been one of the main driving forces for developing fourth-generation light sources. However, it is possible to achieve extremely high coherent electron sources as well. With new phasing routines, atomic level holographic reconstruction has been demonstrated with electrons (Zhang & Zuo, 2009; Huang *et al.*, 2009). Here is one application where the much lower induced damage and higher scattering cross section may give electrons a distinct advantage over X-rays.

At this point, it is important to emphasize that structural dynamics at atomic resolution will require the use of crystals. Irrespective of the reconstruction method, the minimum number of elastically scattered events involves sampling at least 10^6 molecules or unit cells. Rather than try to repeat the experiment one million times for a single time point, it is much simpler to have one million copies of the molecules arranged in a regular manner, *i.e.* in a crystal. Liquids and gas-phase samples can also be used, in which case there is no periodic order to enhance the structural refinement.

2.1. Ultrabright electron-source development

A significant fraction of the atoms or molecules needs to be excited to get the changes in diffraction above the background contributions of the unexcited parts of the sample. In the case of photocrystallography (Coppens, 2003; Techert *et al.*, 2001; Collet *et al.*, 2003; Lorenc *et al.*, 2009), the very act of exciting a crystal normally leads to strain and cracking of crystals due to the induced structural changes. Even without this consideration, the process of laser excitation generally causes changes in the sample through other possible side reactions and non-radiative relaxation mechanisms for energy disposal of the absorbed photon energy into the lattice. It can readily be appreciated that one may quickly run out of sample or film before resolving the motions of interest. The major technological advance that led to the first studies of atomic motions in real time was based on a new concept for creating high-density electron bunches (Siwick *et al.*, 2003).

The major technological challenges to making molecular movies with electron sources are as follows:

(1) Most photoinduced structural changes are irreversible and require sample exchange. Limited sample size puts tight constraints on the number of total possible laser shots. The general solution requires near-single-shot structure determination with atomic resolution.

(2) Near-single-shot structure determinations for reasonable sampling areas require 10^{12} electrons s^{-1} cm^{-2}. At such areal densities, how can we beat space-charge broadening effects on pulse duration to achieve the required sub-ps time resolution?

(3) How can we characterize 100 fs electron pulses? Strong space-charge effects lead to rapidly changing electron pulse durations with propagation. Characterization requires 100 fs time resolution with a spatial resolution along the beam path of 1 mm or less.

(4) How can we characterize $t = 0$ (timing between electron and light pulses) to properly synchronize the films?

The above challenges have been discussed as serious barriers to the use of electron sources for structural dynamics (King *et al.*, 2005). Prior to our work, there was no means to generate pulses with sufficient electron density for near-single-shot structural determinations. Similarly, there was no method to determine the electron pulse duration on the required timescale. In order to have any chance of reducing space-charge effects, the electron-beam size must be on the order of 100 μm and the beam rapidly changes during propagation. Streak cameras only afford 1–2 ps instrument response times for such beam parameters and are not capable of millimetre spatial resolution to characterize high-bunch-number electron pulses. Similarly, there was no means to determine the relative time of arrival of the electron pulse and laser excitation pulse, with the required precision, as needed to synchronize the filming of atomic motions. The effective shutter speed or time resolution of the molecular movie camera is determined by both the pulse duration of the electrons (convolved to the laser excitation pulse) and the accuracy in the $t = 0$ position. It is also necessary to take into account the difference in velocity of electrons and laser light in the sample region as this also affects the instrument response time. If we are to reach the canonical 100 fs time resolution required for making molecular movies as discussed in §1.1, we must be able to fully characterize the pulses with 10–100 fs time resolution and mm spatial resolution along the beam propagation. In the last three years, all of the above technical hurdles have been solved as detailed below.

2.2. Electron-gun design

The experiment requires on the order of 10 000 electrons to achieve near-single-shot conditions. The equations of motion for the electrons interacting through repulsive Coulombic forces were solved numerically in the classical limit to arrive at an effectively exact solution to the problem. We modeled our experimental parameters using 100 kV cm^{-1} fields extraction for 150 fs electron pulses created in an approximately 100 μm beam size with an initial energy spread of 0.6 eV at birth (Siwick *et al.*, 2002). By modeling the electron bunch as a thin two-dimensional disc (initial dimensions at birth are 10 by 100 μm), it was possible to derive a mean field approximation to the electron propagation dynamics. This analytical expression has been shown to be fairly accurate and gives nice insight into the problem (Reed, 2006). The combined use of time-intensive numerical simulations and analytical calculations helped converge on solutions to the space-charge problem.

The electron pulse with the required number density increases its pulse duration by an order of magnitude within 20 cm of propagation. The obvious solution is to have the electron propagation distance as short as possible. With these calculations we finally figured out the required gun paramenters. The first molecular movie camera, our third-generation electron gun within the parlance of the field, was based on a compact design with approximately 4 cm of propagation distance from the photocathode to sample. This gun design was a significant departure from the seminal work of Mourou and co-workers that introduced pump/electron probe protocols to structural dynamics (Williamson & Mourou, 1984). These first electron sources used low-electron-density pulses with relatively long propagation distances. The challenge in the extremely compact gun designs that we introduced was to keep all the surfaces, not just the photocathode region, free of sharp edges and points of high-voltage breakdown. There were also significant challenges with respect to preventing ions produced during laser excitation of samples from backtracking into the photocathode region. By using small extraction pinholes and photocathode exchange it was possible to minimize this problem to an acceptable level. The highest time resolution to structural dynamics to date has been obtained with our fourth-generation electron gun schematically shown in Fig. 2.

The other very significant feature to come out of the theoretical study (Siwick *et al.*, 2002) that was not anticipated prior to the simulations is that nonrelativistic electron bunches very rapidly develop almost perfectly linear chirps. The space-charge-induced increase in the kinetic energy spread is more than a factor of 100 larger than the initial 0.6 eV energy spread. The initial energy spread is negligible. This means that the energy distribution is determined by the spatial position of the electron in the bunch. In this regard, vacuum is 'dispersive' for nonrelativistic electrons; higher-energy electrons travel faster than lower-energy electrons. As the electrons then propagate, the high-energy electrons separate from the lower-energy electrons to eventually form a linear spatial chirp. This feature of nonrelativistic electron bunches is being specifically exploited now for fifth-generation electron guns that will be capable of sub-100 fs electron pulse durations and factors of 100 more electrons per bunch (Fig. 3). The calculated electron pulse parameters in Fig. 3 are for our specific gun design using a radiofrequency (RF) pulse compression cavity (van Oudheusden *et al.*, 2007). In this case, the calculation is based on a generalized particle tracking code that has been shown experimentally to be fairly accurate (Hebeisen, Sciaini, Harb, Ernstorfer, Dartigalongue *et al.*, 2008). All the results to be presented in this review will be improved by more than a factor of 10^3 with these new gun designs and every-electron

detection that will compete head to head with fourth-generation light sources on many problems. In this regard, there will be some problems better suited to study with electrons and some with X-rays.

2.3. Pulse characterization

As can be readily appreciated from even a cursory inspection of Fig. 3, high-number-density electron pulses rapidly change with propagation distance. Until recently, it was not possible to characterize electron pulses on the 10 fs timescale now approachable with fifth-generation electron guns nor could one make such measurements with the required sub-mm spatial accuracy.

We were able to solve this problem using the laser ponderomotive effect to spatially deflect electrons. This scattering process provides a mechanism to cross-correlate an unknown electron pulse with a known laser pulse to both determine the electron pulse duration (or shutter speed of the camera) and $t = 0$ position that is essential to the accurate determination of decay components in the material response (or synchronizing the film).

Scattering of electrons by light was first proposed by Kapitza & Dirac (1933) and realized in 1988 using 20 eV electrons and a pair of counter-propagating 100 ps laser pulses (Bucksbaum *et al.*, 1988). While the cycle-averaged force on an electron in a plane wave is zero, this is not the case in a laser field with an intensity gradient (Kibble, 1966). In such an inhomogeneous laser field, an electron experiences a force

$$\mathbf{F} = \frac{-q^2\lambda^2}{8\pi^2 m\varepsilon_0 c^3}\nabla I, \qquad (1)$$

i.e. the electron experiences a force away from regions of high intensity (I). Here, q is the elementary charge, λ is the wavelength of the laser, m is the electron mass and ε_0 is the permittivity of vacuum. This force is called the ponderomotive force. Since the ponderomotive force is only present when the light is present, a passing fs laser pulse creates a pulsed force field only for the laser pulse duration. Therefore it can be used to selectively scatter a short section of an electron pulse and, by varying the time delay between the laser and electron pulse, map out the electron temporal profile (Hebeisen *et al.*, 2006).

Simulations using an n-body tree code, which took the laser ponderomotive force of a strong fs laser pulse into account, showed that it is possible to scatter the electrons of a fs electron pulse enough to significantly change the distribution of electrons on the detector. Fig. 4 shows a dramatic capture of the electron pulse in free flight to illustrate how well this method works.

This measurement is nontrivial and requires a major laser facility to deliver 10–100 fs laser pulses in the 10 mJ range. We have recently greatly improved the method. By using two laser

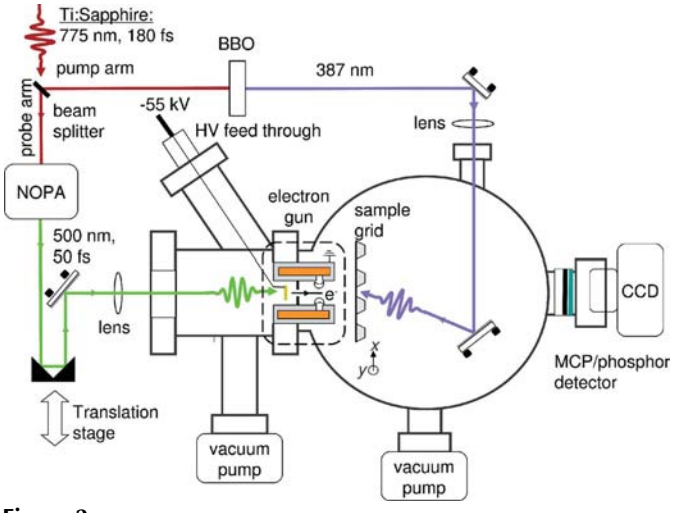

Figure 2
General experimental layout for fs electron diffraction. The laser beam of a Ti:sapphire regenerative amplifier (775 nm, 180 fs) is split into two beams. One of them passes through a β-$Ba_2B_2O_4$ (BBO) crystal for second harmonic generation (SHG). This beam induces structural changes in the sample (pump pulse). The other part of the 775 nm beam is redirected to a noncollinear optical parametric amplifier (NOPA) to produce 500 nm 50 fs pulses. Electrons are generated *via* two-photon photoemission from an Au photocathode and accelerated to 55 keV over a distance of 6 mm, *i.e.* with an electric field close to the vacuum breakdown limit of ~10 MV m^{-1}. This electron beam is the probe pulse of the experiment. A magnetic lens focuses the electron beam prior to scattering off the free-standing films at a distance of approximately 3 cm from the photocathode (at this position the typical energy spread is approximately 0.1%). The diffraction pattern is detected by a microchannel plate (MCP)/phosphor screen and recorded with a charge-couple device (CCD) camera. The experiment is carried out under a high-vacuum environment with a base pressure of ~10^{-7} mbar (1 mbar = 0.1 kPa).

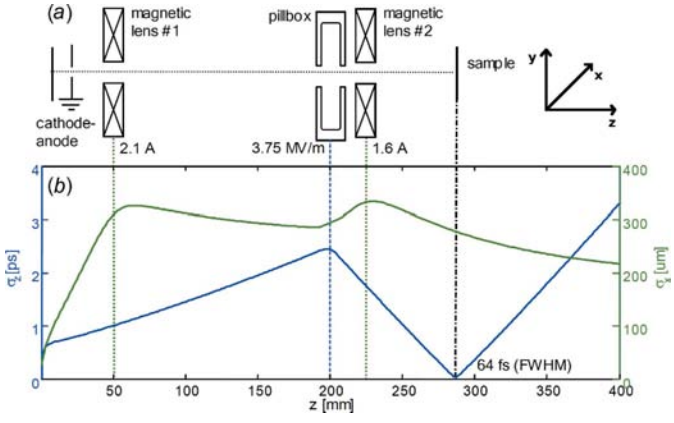

Figure 3
Fifth-generation electron guns. (*a*) Schematic of the electron pulse compression system. The basic concept involves the use of an RF cavity to invert the velocity chirp acquired during space-charge broadening during pulse propagation. The RF field in the box marked pillbox is such that the front edge of the pulse sees a smaller electric field than the back edge as the RF field of approximately 3 GHz frequency changes enough during the pulse propagation through the lens to invert the so-called phase space (momentum:position) of the electron pulse. (*b*) Simulations of the pulse propagation dynamics performed using the *General Particle Tracer* (*GPT*) code (http://www.pulsar.nl/gpt/) show the evolution of the beam size (green) and the pulse duration (blue) as the pulse traverses the different elements. The electron pulse is effectively time focused to a minimum pulse duration (at 285 mm) where the sample needs to be located. Note the rapid change in pulse duration with propagation. It is necessary to characterize the pulse with 10–100 fs time resolution and mm spatial resolution [for details see Harb (2009)].

pulses in a counterpropagating beam geometry (see Fig. 5) to make a standing intensity grating, we have enhanced the intensity gradient enormously [see equation (1)] and increased the number of scattering centers (Hebeisen, Sciaini, Harb, Ernstorfer, Dartigalongue *et al.*, 2008). Each fringe in the interference grating represents a scattering center. This configuration increases the laser ponderomotive scattering efficiency by approximately a factor of 100. These measurements are now routine and can be conducted with μJ pulsed systems. This reduces the laser requirements to conduct atomically resolved structural dynamics to that of a tabletop fs amplified fiber laser system. Fig. 5 shows representative data acquired with this approach (Hebeisen, Sciaini, Harb, Ernstorfer, Dartigalongue *et al.*, 2008). Comparison of electron pulse durations measured with this scheme with results from *n*-body simulations of electron pulse propagation dynamics shows that not only can we fully characterize electron pulses but we can also very accurately model the electron propagation dynamics for optimally designing electron guns for structural dynamics.

The above discussion documents the historical path to high-intensity electron sources that are now capable of 10–100 fs time resolution, sufficient to capture the fastest atomic motions, and most important with sufficient intensity for single-shot structure determinations. These advances have been discussed for nonrelativistic electrons as only these sources have demonstrated fs time resolution with sufficient number of diffraction orders to retrieve structural dynamics to date. There are equally promising developments based on relativistic electron sources (Hastings *et al.*, 2006; van der Geer *et al.*, 2007) but these machines have not been employed in time-resolved measurements as yet. All the technical hurdles to making a molecular movie camera based on nonrelativistic electron diffraction have been overcome. These technical advances have served as the basis for the first atomically resolved structural dynamics that qualify as a molecular movie (Siwick *et al.*, 2003).

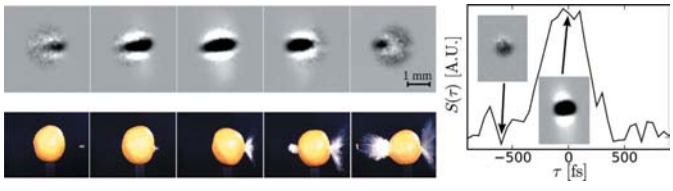

Figure 4
Capturing an electron bullet in free flight. The top left panel shows the passage of a 15 mJ laser pulse of 90 fs duration through an electron pulse at time steps of approximately 100 fs. The electron beam ultimately impinges on an MCP detector/phosphor detector for imaging. The observations show directly that the electron pulse is comparable in duration to the 90 fs laser pulse. For effect (bottom left), this rendering is compared to a time-sequence of photographs of a bullet passing through a lemon (courtesy Andrew Davidhazy, RIT). Right panel, an example pulse profile is quantified by correlating the defected electron density as a function of relative delay between the electron pulse and the laser pulse used as the ponderomotive scattering source (Hebeisen *et al.*, 2006).

The tools are now in place for generating and fully characterizing fs electron pulses. Just as in fs optical studies with the advent of nonlinear correlation methods, it is *no longer acceptable to estimate electron pulse durations* or time resolution based on material responses with unknown time lags. *Pulses need to be fully characterized and the instrument response function needs to be accurately reported*.

3. The science: first frames

3.1. Atomically resolved phase transitions

As with any new method, one starts with the simplest systems for study first. In terms of structural dynamics, one of the simplest structural changes is melting. Everyone has experienced this phenomenon first hand. This is an order-to-disorder phase transition. The simple question is how does something go from an ordered structure such as a face-centered cubic (f.c.c.) lattice with a coordination number of 12 to the disordered shell-like structure of a liquid? The length scales of motion, collapse of the transverse barrier to highly anharmonic liquid motion and rearrangement to a shell-like liquid structure depend on how strongly driven the phase transition is.

To make the problem a little more graphic, we all know how ice melts. If you imagine a block of ice melting, you know it melts from the surface inwards. The melting point of the surface layer is lower than the bulk and the temperature

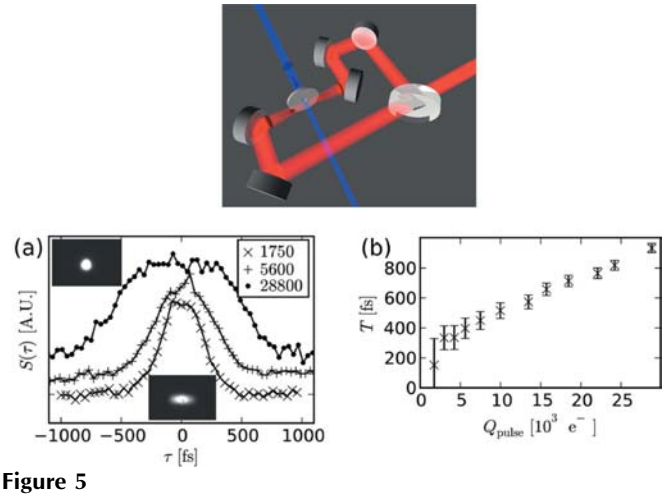

Figure 5
Top: experimental layout for the grating-enhanced ponderomotive scattering experiment. The laser pulse (red, entering from the right) is split into two parts by a beam splitter. The two pulses propagate along matched paths to collide in the electron beam path, forming a transient intensity grating. The electron pulse (blue, entering from the top) is stripped of its outer electrons to better match the laser focus size just before the crossing point with the laser pulses. In practice, the laser beam is focused by a lens placed before the beam splitter. Bottom: (*a*) electron pulse–laser pulse cross-correlation traces obtained by grating-enhanced laser ponderomotive scattering of electrons for different numbers of electrons per pulse (vertical offset added for clarity). The inset pictures show images of the electron beam on the detector. The propagation direction of the laser pulses is horizontal and the electrons are scattered along the laser propagation. (*b*) Measured electron pulse duration *versus* number of electrons per pulse (Hebeisen, 2009).

gradient exists at the ice interface. So melting occurs at the interface and propagates inward in a process known as heterogeneous nucleation. At a pressure of 1 atm (101 325 Pa), the inwardly propagating liquid melt zone is fixed at a temperature of 273.15 K. The other bit of information gained from everyday experiences is that if we were to increase the rate of heating of the ice it would melt faster. If a blow torch was directed towards the ice, the melt zone would propagate inward to the bulk faster. The temperature of the melt zone would still be 273.15 K at 1 atm. There is, however, clearly a relation between the rate of heating and the propagation of the melt zone that can be described mathematically. Now here is the other intriguing question. What if we had a special kind of 'blow torch' with which we could heat up the ice so fast that no matter what theory you used, you would predict the ice would melt faster than the atoms could move? This question was pondered by Born, among others, back in the 1930s with respect to the fleeting state of superheated matter (Born, 1939). At some point, the granularity of the interatomic potential should factor into the problem. Now, in a manner of speaking, we do have a special kind of 'blow torch'. With fs lasers, it is possible to deposit energy into a lattice and have it thermalize at heating rates of 10^{15} K s^{-1}. We can approach this intriguing speed limit to examine how fast materials can lose structural correlations.

There is another important consideration with the application of fs laser pulses with respect to exciting materials. It has been determined that there is a unique and special attribute to fs laser excitation, not seen with longer pulses. If the laser pulse excites approximately 10% of the material's electrons, most materials will appear to melt on timescales faster than the absorbed energy can be thermalized. This process is referred to as electronic induced melting or nonthermal melting. With longer pulses, the energy is thermalized faster than material excitation so this effect is not observed. Basically, on the fs timescale the lattice is frozen. The use of fs excitation creates a new charge distribution that alters the bonding, generally softening the lattice. At some point the lattice potential is no longer a bound state and the lattice appears to 'melt' from various optical signatures (see §3.3).

The notion of nonthermal melting has never been rigorously tested with structural probes. The observation of so-called nonthermal melting has always been done through changes in the frequency dependence of the material linear and nonlinear susceptibility or optical properties. Under such strong electronic excitation, these parameters are not well known. The effect of nonthermal melting could simply be disordering of the periodic electronic structure describing the valence electrons or population of uncorrelated excited states in a molecular basis that leads to the changes in optical properties. Irrespective, the use of fs laser pulses to change the charge distribution within an initially frozen lattice description allows the manipulation of interatomic forces and energy landscapes of materials. It is this aspect of fs-laser-driven phase transitions that is so intriguing. The timescale is so short that we can literally go into the material, rearrange the electron distribution and watch how this affects the fundamental forces of bonding. To access this information, we need to directly observe the atomic motions in response to the induced change in bond strength. This problem was the first to be addressed using structurally sensitive probes with sufficient time resolution to observe the relative atomic motions faster than collisional blurring of the time-dependent atomic pair correlations and information on the induced changes in bonding.

At the time of these experiments, our group was inspired to study the issue of nonthermal melting of aluminium by the work of Guo *et al.* (2000). They observed what appeared to be the onset of nonthermal melting for absorbed excitation fluences corresponding to approximately 1.5 times the energy required to melt the lattice or a superheating parameter (θ) of 1.5. Under these excitation conditions, the lattice optically appeared to take on the dielectric properties of liquid Al within 600 fs. This conclusion was based on observing the changes in optical reflectivity at various angles for a single color and comparison of the derived parameters to that of liquid *versus* solid Al. This observation was remarkable in that Al is viewed as the classic jellium-like metal. The crystal structure of Al is f.c.c. with no directional bonding, *i.e.* the band structure can be well described by an isotropic distribution of electrons bound by the collective periodic potential of the underlying positively charged nuclei. The melting of Al within 600 fs is also remarkable in that this nominally isotropic electron distribution would have to lead to statistical variations leading to bond breaking on a timescale of just a few phonon periods or effective lattice collisions. How is this possible?

3.2. Thermally driven phase transitions in free electron metals

The basic idea of nonthermal melting is that the optical excitation leads to an interband transition in which the upper-level band structure has more antibonding character and involves weaker bonds. At excitation levels of approximately 10% of the valence electrons, the lattice is no longer a bound state and it collapses to a disordered structure through a purely electronic effect. This concept can be readily understood by considering the simple quantum particle-in-a-box problem. In going from one level to the next higher level, the nodes in the electron's wavefunction increase by one. The same effect occurs for all electronic wavefunctions. This effect would deplete electron density between atoms and reduce the effective increase in nuclear attraction induced by sharing of electron density, *i.e.* decreases the bond energy. However, what is unusual for Al is that there is no directional bonding. So why would the change in electron distribution affect bonding? Also, in considering the electron excitation process, the excited electrons would have to remain in the new electron distribution corresponding to the initially accessed electronic band for this degree of antibonding or bond softening to persist. However, the electron–electron scattering rate with the underlying cold, unexcited electrons is exceedingly fast in metals, faster than the reported 600 fs.

It is apparent that this problem contains some deep fundamental issues. First, the use of fs laser pulses to rearrange electron distributions within a frozen lattice allows us to explore the fundamental connection between electron distribution and bonding. In order to access this information we need to directly observe the atomic motions in response to the induced changes in the potential energy surface of the lattice to report on the changes in forces. The new ability to directly observe atomic motions on the prerequisite timescale and spatial resolution using fs electron diffraction (FED) opens up this possibility. Prior to this development, we could only measure material properties as given. Now we can manipulate electron distributions and observe the change in bonding. In principle, studies of optically induced changes in the phonon dispersion could give this information but the optical phonons typically become strongly damped at such excitation conditions and the entire phonon branch would have to be determined to invert to changes in the lattice potential energy surface. This information is obtained directly from the determination of the displacement of the atoms from their equilibrium positions. In addition, this class of experiments enables us to probe electron–electron correlation effects. We have deeply ingrained views of lattice structure in terms of an atomistic view. However, the minimum energy position giving rise to this structure is related to the minimum energy for a given electronic distribution or electronic state and this is a true many-body effect. We can now view the consequences of electron–electron correlations as will be described below.

The first experimental study of structural dynamics to achieve sub-ps time resolution, as required to solve a problem, is shown in Fig. 6. These studies were conducted under the exact same excitation conditions used in the optical studies that reported nonthermal melting of Al (Guo *et al.*, 2000). The results are rather dramatic and do not need a high level of analysis to arrive at the most important conclusions of the work. It is immediately apparent that the crystal still shows diffraction from long-range order at an electron probe delay of t = 500 fs. At t = 1.5 ps, the higher orders of diffraction indicative of the solid-state order are still present but dimmer. This decrease in diffraction from the higher diffraction orders is due to a well known effect of lattice heating and a decrease in coherence of the diffraction process, or Debye–Waller effect. The larger r.m.s. atomic motions decrease the correlation in atomic positions and thus lead to decreases in constructive interference leading to diffraction at a given order. The amplitude of the higher-order diffractions falls off quadratically with scattering wavevector. This effect is used to determine the amplitude of r.m.s. atomic motions and lattice heating dynamics. It is not until t = 2.5 ps that one sees the onset of the diffraction at low scattering wavevectors indicative of liquid formation. At t = 3.5 ps, it is apparent that the entire sample has been converted to the liquid state. Based on this simple pattern recognition of the general features of solid state and liquid state, one can arrive at one of the most important conclusions of this work. The solid-to-liquid phase transition is not nonthermal but rather can be completely understood as a thermally driven phase transition. The melting dynamics occur on the ps timescale and not the hundreds of fs timescale required for a purely electronically driven process. In addition, it is clear that the nucleation process and lattice collapse occur with a propagation time across the entire sample of less than 2 ps. This propagation time is faster than the speed of sound (getting back to our original question). For a 20 nm-thick sample, it would take at least 8 ps for the melt zone to propagate through the sample at the speed of sound if it was to occur through heterogeneous nucleation. The mechanism of melting clearly involves homogeneous nucleation, it is melting from the inside–out in contrast to melting from the outside–in as in the normal heterogeneous nucleation process. The degree of superheating (θ = 1.5) is such that there is enough thermal energy to overcome barriers to forming liquid nucleation sites. The nucleation sites must be on the order of nm to not subtend the whole sample, *i.e.* the nucleation sites are truly molecular in scale.

The transition to the liquid state can be seen more clearly by looking at the difference diffraction data and comparing the

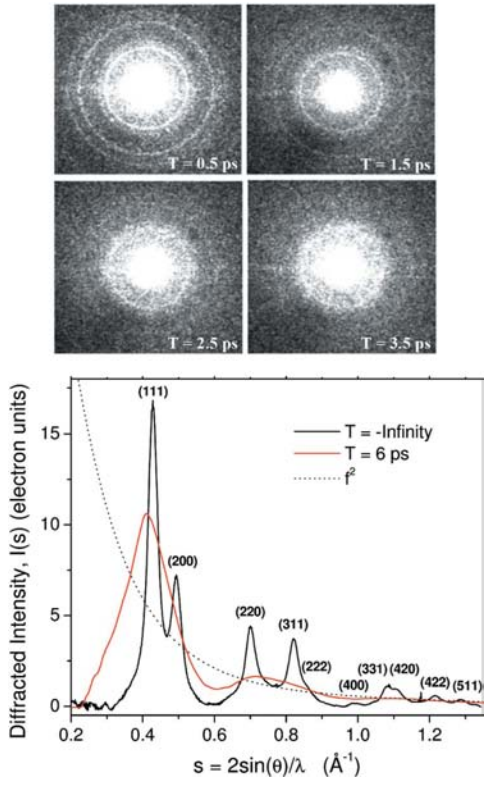

Figure 6
First frames. The top panel shows the raw electron diffraction data for polycrystalline Al under excitation conditions corresponding to a superheating of approximately 1.5. The polycrystalline sample gives the classic ring structure for diffraction from randomly oriented crystal projections. The long-range solid-state order is clearly visible up to 1.5 ps time delays after the excitation pulse through the higher-order diffraction rings. Between 2.5 and 3.5 ps, the lattice is seen to collapse to the shell-like diffraction pattern with intensity build-up at low scattering wavevectors corresponding to the shell-like structure of liquids. The bottom panel shows the radially averaged data and peak assignments. The data shown for 6 ps illustrate that the diffraction is from liquid Al. The signal did not signficantly change between 3.5 and 6 ps (Siwick *et al.*, 2003).

decay in the high-order diffraction intensities with expected lattice heating effects. The build-up of diffracted electron density at low scattering wavevector (s) indicative of longer-range density changes in forming a liquid structure is apparent. The analysis of the data clearly shows a thermally driven phase transition with an abrupt collapse to the liquid state in which large-amplitude thermal motions ultimately lead to bond breaking and creation of liquid-state nucleation sites (Siwick *et al.*, 2003). Once the nucleation sites form there is very rapid collapse of the entire lattice. Here the importance of obtaining a sufficient number of diffraction orders to invert the diffraction to structure needs to be emphasized. Previous time-resolved diffraction experiments of the melting phase transition were only able to resolve a single rocking curve for a particular diffraction order (Rousse *et al.*, 2001; Siders *et al.*, 1999; Cavalleri *et al.*, 2001). These early studies did not have the brightness sufficient for more orders. In this regard, it is important to point out that if we did not have enough source brightness and could only examine the (111) diffraction order we would have concluded the sample did not melt. This peak overlaps with the liquid peak and only decays to a common amplitude. In contrast, if we were to monitor the highest-order diffractions, (331) or (420), we might have concluded that the lattice was undergoing nonthermal melting as the decay in amplitude is sub-ps. The decay in this order nicely demonstrates that the time resolution of this experiment was in fact in the hundreds of fs range (600 fs instrument response) as required to resolve the issue of thermal *versus* nonthermal melting. The main point here is that multiple diffraction orders are needed to invert to structure.

The need for structure-sensitive probes such as electron or X-ray diffraction has been made apparent in these studies. It is simply not possible to connect changes in optical properties, over a limited frequency spectrum, to structure. There needs to be significant theoretical modeling of the correlation between changes in spectra and structure. This statement holds true for all frequency ranges. It is possible, however, to use a very broad spectrum to access multiple transitions to discern collapse of band structure and give qualitative statements about the process. The electron diffraction studies have been further confirmed by such a broadband spectral analysis that shows melting occurring on a 2 ps timescale indicative of a thermally propagated phase transition (Kandyla *et al.*, 2007).

A more detailed analysis of the actual mechanics in the disordering process can be gleaned from the diffraction data by inverting from reciprocal space to the reduced density function (Siwick *et al.*, 2003).

This study represents the first to attain enough diffraction orders with sufficient time resolution to provide a real-time picture of atomic motions on timescales faster than collisions and the onset of diffusive motions that wash out the details. It is exactly this kind of picture we would like to obtain for functionally relevant protein motions. In this latter case, the process would retain some overlying order. We would know the effective mass of the displacements and the time-dependent velocities or forces. This information can be inverted to give the principal components of the potential energy landscape, encoded in the protein structure, that is responsible for function. The work on Al is the first step towards this objective.

Since this initial work, a number of other systems have been explored for different band structures. Fig. 7 is intended to show the effect of strong electronic excitation on the interatomic potential in the systems discussed in the next sections.

3.3. Electronically driven phase transitions in semiconductors

The prospect of inducing changes in bonding due to electronic excitation was first suggested by time-resolved second-harmonic-generation measurements of Si by Shank *et al.* (1983). In this study, Si appeared to develop liquid-like properties within 240 fs, a timescale which is effectively just a few phonon periods. The notion that one could excite material and cause it to undergo a phase transition by manipulating the chemical bonding was intriguing. The initial experimental observations were backed up by theoretical predictions of lattice collapse at excitation levels corresponding to ~10% of the valence electrons (Biswas & Ambegaokar, 1982; Dumitrica *et al.*, 2003; Stampfli & Bennemann, 1994). The nature of the perturbed lattice potential, and the mechanism by which the lattice disorders, however, remained an open debate.

In order to gain more insight into this problem, several studies attempted to resolve the dynamics of the disordering process by directly probing transient structure using X-rays (Rousse *et al.*, 2001; Siders *et al.*, 1999; Cavalleri *et al.*, 2001). These initial studies constituted an important proof-of-principle but were nevertheless limited in time resolution and SNR. A more recent study by Lindenberg (2005) used the X-ray beamline at Stanford's Sub-Picosecond Pulse Source (SPPS) facility to investigate electronically driven atomic motions in another semiconductor, namely InSb. A number of diffraction orders and rocking curves were sampled following intense optical excitation. Based on the extracted timescales, these authors concluded that the atoms had moved inertially from their initial positions at their initial room-temperature

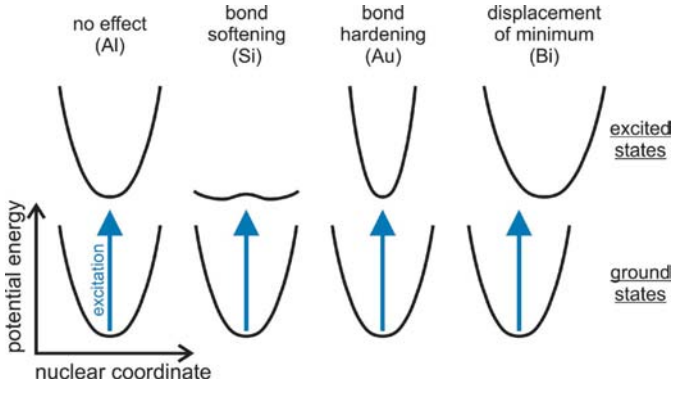

Figure 7
Schematic illustration of the possible effects of strong electronic excitation (indicated by blue arrows) on the potential energy surfaces in different materials. These qualitatively different effects are manifested in the dynamics of strongly driven phase transitions.

velocities. It was postulated that the bonds had been effectively snipped and the atoms moved freely within an optically induced, flattened potential characteristic of the liquid state. This process occurred within ~300 fs. We note, however, that the inertial dynamics picture has been recently disputed by a theoretical study (Zijlstra *et al.*, 2008).

With the development of our fourth-generation electron gun, we were able to reduce the electron pulse duration to 200 fs to provide enough time resolution to study this problem in Si. We also developed Si nanofabrication methods to make a large sample array of 50 nm free-standing polycrystalline Si membranes (Harb *et al.*, 2006). Given the destructive nature of the excitation, this development allowed us to average multiple sample points per time step to improve the SNR. We were also able to further increase the SNR by using single-crystalline Si (Harb *et al.*, 2008). Fig. 8 shows the decay of the (220) diffraction order of (001)-oriented single-crystalline Si at an absorbed fluence of 65 mJ cm^{-2}, equivalent to the excitation of 11% of the valence electrons. The decay of crystalline order was accompanied by a rise in the intensity of the diffraction signal in the scattering range corresponding to the diffraction profile of liquid Si (Kita *et al.*, 1994). Both kinetics (decay of order and rise of disorder) occurred on the same ~400 fs timescale. Therefore, as theoretically predicted, Si did indeed 'melt' on a timescale indicative of electronically induced bond softening. Additional experiments were performed with polycrystalline Si samples and several diffraction orders probed. Rather than showing a quadratic dependence in the decay time with scattering vector if the process was concerted, each diffraction order showed the same decay profile. Such an observation suggests that the diffraction from the different orders indicates the fraction of solid-state lattice remaining as a function of time.

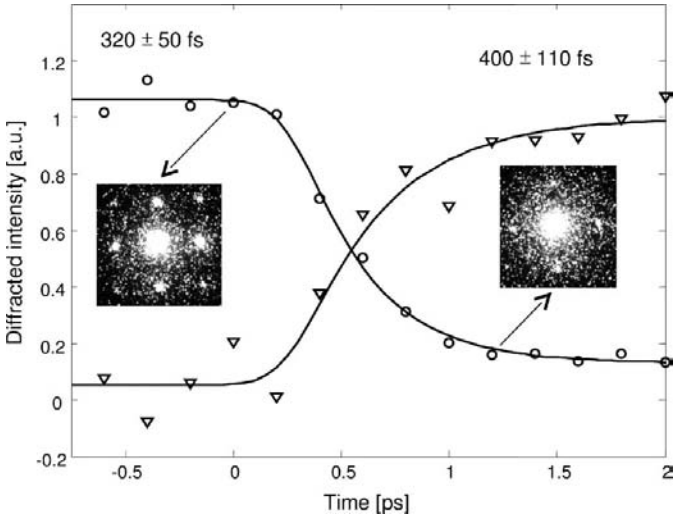

Figure 8
Electron diffraction kinetics of the (001)-oriented single-crystalline Si sample excited with 400 nm light at an absorbed fluence of 65 mJ cm^{-2}. The diffracted intensity of the (220) peak (circles) was found to decay in 320 fs as determined by a fit of an exponential decay function convoluted with the ~300 fs instrument response time. The diffracted signal in the 0.22–0.60 Å^{-1} scattering range (triangles) was found to develop on a similar timescale (400 fs). The two images shown inside the panel are snapshots of the diffraction pattern taken at 0 ps (left) and +1.2 ps (right) following excitation.

Here we need to make an important distinction between this work and the InSb studies. A liquid does not have a flat potential energy surface as asserted for InSb. Rather, it is a bound state of matter with small barriers separating local configurations that rapidly interconvert. The key distinguishing feature of the liquid state is its inability to support shear motions, or collapse of the transverse acoustic branch of the corresponding solid-state phase. This occurs when the system has enough thermal energy to overcome the barriers within the potential energy surface to shearing motions. It was exactly this class of motions in the Al studies that led the system from a coordination number of 12 for the f.c.c. lattice to the liquid shell structure with an average coordination number of 10 (Siwick *et al.*, 2003). The interesting feature of the observation for Si is that it is the first direct observation of electronically induced nucleation centers. There will be electronically induced lattice instabilities that lead to nucleation sites, as in the thermally sampled case of Al, but on a much faster timescale. Also, and more intriguing, one has to consider the fluctuating electron–hole carrier distribution in the process. The photoexcited electrons will be rapidly exchanging spatial positions through various scattering mechanisms at high excitation. There will be regions with higher densities of conduction band electrons and this will lead to additional lattice softening. The highly directional nature of the bonding in Si is ultimately responsible for the electronically induced bond softening, and breaking with the background ambient thermal energy. The increased antibonding character of the photoinduced charge distribution necessarily takes the system to a softer potential. The changes in charge distribution introduce potential gradients or forces displacing the atoms from the equilibrium minima and propagate the system on to a rapidly fluctuating liquid potential energy surface.

These particular studies are important in that Si owes its special properties to its highly directional bonding and associated diamond-like structure. This work showed that we could optically manipulate the lattice potential for such a well defined system. We now have the ability to manipulate electron density and directly observe the effect on chemical bonding. This class of experiments will rigorously test various approximations made in first-principle calculations of Si and serve as an important benchmark for further development of time-dependent methods for treating structural dynamics.

3.4. Electronic bond hardening in gold: applications to extreme physics

In stark contrast to the photoinduced bond softening in semiconductors, the opposite effect has been theoretically predicted for gold. Based on *ab initio* calculations, the stability of a cool gold lattice increases with increasing electron temperature (Recoules *et al.*, 2006; Bottin & Zerah, 2007). According to these calculations, intense electronic excitation leads to a transient increase of the melting temperature, which alternatively can be expressed as a transient increase of the

Debye temperature. Therefore, the effect of electronic bond hardening manifests itself in the kinetics of the order-to-disorder phase transition. The electron temperatures required to induce bond hardening are in the range of a few eV, which corresponds to energy densities of several MJ kg^{-1}.

Fig. 9 shows the electron diffraction signal of a gold film before and 50 ps after intense optical excitation. At the latter time, the excitation energy equilibrated within electronic and nuclear degrees of freedom and a dense plasma, often referred to as warm dense matter, has formed. The transition from crystalline gold to a disordered state is characterized by a complete loss of all Bragg peaks, the formation of a single diffraction feature characteristic of a liquid-like state and an overall increase of diffuse scattering. The evolution of the nuclear structure after absorption of 2.85 MJ kg^{-1} with a 200 fs pump pulse is shown in the right panel of Fig. 9 as a function of the relative change of the Debye–Waller factor (DWF) of the (220) diffraction. Despite the high excitation level, the Bragg peak decays surprisingly slowly with a time constant of 1.9 $\pm$ 0.2 ps (Ernstorfer *et al.*, 2009). Fig. 9 also shows the simulated time dependence of the (220) peak based on a two-temperature model (TTM) by Lin *et al.* (2008). In contrast to previous TTMs, these authors explicitly treat the material-specific electron temperature dependence of the electron heat capacity and of the electron–phonon coupling. This model does not take into account the effect of bond hardening and predicts a decay of the (220) Bragg peak with a clear deviation from the experimental data, as indicated in Fig. 9. However, modification of the model by introducing electronic bond hardening *via* an electron-temperature-dependent Debye temperature according to Recoules *et al.* (2006) results in very good agreement between simulation and experiment. This agreement is a clear indication of an electronically hardened lattice with a transiently increased melting temperature.

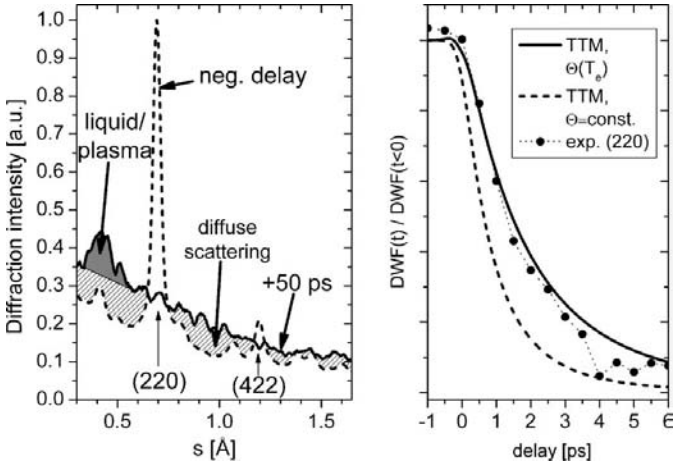

Figure 9
Left panel: electron diffraction signal of a 20 nm-thick free-standing 111-oriented polycrystalline gold film before (dashed line) and 50 ps after (solid line) optical excitation. Right panel: time-dependent diffraction intensity of the (220) Bragg peak (dots) and simulated decay of the (220) intensity with two-temperature models including (solid line) and excluding (dashed line) the effect of bond hardening. Excitation level: 2.85 MJ kg^{-1}.

Furthermore, the dynamics of melting is a direct measurement of lattice stability. At lattice superheating of 1.5, the dynamics for melting were well described by atomistic MD simulations of the melting. Subsequent increases in the degree of superheating with such a basis should lead to supra-linear melting dynamics, *e.g.* increasing the degree of superheating by 2 should lead to the onset of melting more than twice as fast. In contrast, as we increased the degree of superheating, the time for the onset of melting slowed down relative to this predicted trend. The sublinear dependence of the melting dynamics on excitation or electronic temperature is another indication that the lattice is getting stiffer or experiencing bond hardening. The lattice potential is significantly stiffened by the reduced nuclear screening of the higher excited electrons (Recoules *et al.*, 2006; Bottin & Zerah, 2007).

Based on atomistic potentials, such an effect should not be observed. This lattice stiffening at high electronic temperatures is clearly a many-body effect. The simplest example we can provide to give some insight to the operating physics is to consider the bonding in diatomic oxygen. Threshold photoionization of O_2 would remove an electron from the highest lying molecular orbital that is antibonding and is responsible for the bond order of O_2 being 2 instead of 2.5 as in the case of O_2^+. Excitation to a higher orbital would similarly decrease the antibonding character or screening of the π molecular orbital and lead to bond stiffening. In the case of Au, the effect is more complicated as it involves correlated electron motions of a large number of electrons per atom center. However, the basic physics behind the bond-hardening effect is similar. The total energy of the system has increased. It is still a higher excited state of matter. It is just that the energy resides in the electron degrees of freedom at the expense of the lower lattice potential energy. In addition, this work has illustrated that it is possible to use fs excitation pulses to manipulate potential energy landscapes. In this case, we have shown that we can make the lattice stiffer or increase the depth of the valleys in the interatomic potential. We have likely also increased the barriers to nucleation in the process that would also have contributed to the retarded melting dynamics at high electronic temperatures.

To give a different perspective on this problem, we did not know what the state for warm dense matter was prior to this work. It was not clear whether it was best to describe this as liquid, a high density of interacting ions or pre-plasma state, or some other description of the mass–charge distribution. At the excitation levels used, the electrons and nuclei eventually equilibrate with temperatures on the order of 10 000 K. Given the surface temperature of the sun is about 5000 K, it was as if we reached into the sun (if it was made of Au) and pulled out a handful of material from below the surface, examined it and found it to be in the liquid state. We now know what state Au is under these rarefied conditions. In our hands, these are fleeting states of matter; yet their properties are highly relevant to the extreme physics key to understanding important phenomena ranging from planetary physics to fusion

processes as an energy source. Until the development of structural probes with fs time resolution, it was not possible to fully characterize these states of matter. At higher excitation levels yet, we can also characterize the spatial distribution of charge as the system evolves into a plasma state by using electron pulses to image field lines (Hebeisen, Sciaini, Harb, Ernstorfer, Kruglik & Miller, 2008). FED seems very well suited to significantly advance our understanding of warm dense matter and extreme physics.

3.5. Photodriven relaxation of Peierls distortions in Bi: approaching the speed limit for atomic motions

The possibility of manipulating bonding, as discussed above, has been one of the dreams pursued by chemists and physicists. In this context the use of ultrashort optical pulses for controlling dynamical processes and chemical reactions with light has been extensively exploited (Shapiro & Brumer, 2003). In general, for systems with a reduced number of degrees of freedom, such as small molecules in the gas phase (Bernstein, 1982), the absorption of a photon in the UV–visible range leads the system to a higher electronic state and, therefore, it evolves according to the forces implied by this new potential energy surface (PES). If the optical pulse is short enough and the molecular ensemble presents a well defined initial equilibrium state, all photoexcited molecules in an ensemble can, in principle, be prepared in a very similar quantum state for them to evolve *coherently*, *i.e.* in a vibrational wave-packet fashion (Rice, 1992). Beyond this weak-field approximation limit, the use of strong fields has also been exploited to coherently control bond excitation (Weinacht *et al.*, 1999). The use of strong laser fields can substantially alter the molecular dynamics up to the point where conical-like intersections are induced in the PES.

For the molecular systems mentioned above the photoexcitation process is well localized, *i.e.* within each molecule; however, light–matter interaction becomes more complex in extended systems. Crystalline systems such as metals (Nie *et al.*, 2006; Siwick *et al.*, 2003; Ernstorfer *et al.*, 2009), semiconductors (Siders *et al.*, 1999; Lindenberg, 2005; Harb *et al.*, 2006, 2008; Zijlstra *et al.*, 2008) and high-T_c superconductors (Carbone *et al.*, 2008) have been studied by FED and fs X-ray diffraction. The photophysics of extended systems is very different from that of simple molecules in the gas phase by virtue of the highly delocalized electronic states that contribute to the lattice potential. Electronic delocalization is the key starting point for electron–electron and/or electron–lattice correlations to play any role in governing collective properties. Strongly correlated systems have received considerable attention since the revolutionary Bardeen–Cooper–Schrieffer theory of superconductivity (Lundqvist & Lundqvist, 1973).

In this regard, Bi is a strongly correlated system that exhibits many exotic effects that range from huge magnetoresistance (Yang *et al.*, 1999), large-amplitude coherent optical phonons (Sokolowski-Tinten *et al.*, 2003; Fritz *et al.*, 2007) and squeezed phonons (Johnson *et al.*, 2009) to electron fractionalization in the ultraquantum limit (Behnia *et al.*, 2007). Bi possesses a Peierls-distorted crystalline structure, known as A7 arsenic type, which can be derived by distorting the cubic NaCl structure (Peierls, 1991; Madelung *et al.*, 1998). This effect makes Bi experience a rather complex coexistence of metallic and covalent bonding (Madelung *et al.*, 1998).

Owing to the strong coupling between electronic and nuclear degrees of freedom, moderate electronic excitation causes the system to evolve towards the symmetric configuration. Thus, upon photoexcitation, the PES minimum shifts, leading to the excitation of large-amplitude coherent A_{1g} phonons. Those PES changes along the A_{1g} mode, *i.e.* longitudinal direction, were monitored by fs X-ray diffraction (Sokolowski-Tinten *et al.*, 2003; Fritz *et al.*, 2007) for excitation levels below the threshold for irreversible damage of the Bi films. Theoretical studies based on density functional theory (DFT) calculations predict that, with increasing excitation, the A_{1g} phonon mode softens to later stiffen for excited carrier densities >2.5% (Murray *et al.*, 2005). Calculations in a two-dimensional space, up to an excitation level of 1.5%, have shown that the E_g phonon mode (transverse mode) flattens with the increase of the photoexcitation fluence (Zijlstra *et al.*, 2006*a*,*b*). In order to examine further the PES evolution and experimentally test these predictions, we performed FED experiments under strongly nonreversible conditions, *i.e.* well beyond the melting point of Bi (Sciaini *et al.*, 2009). During

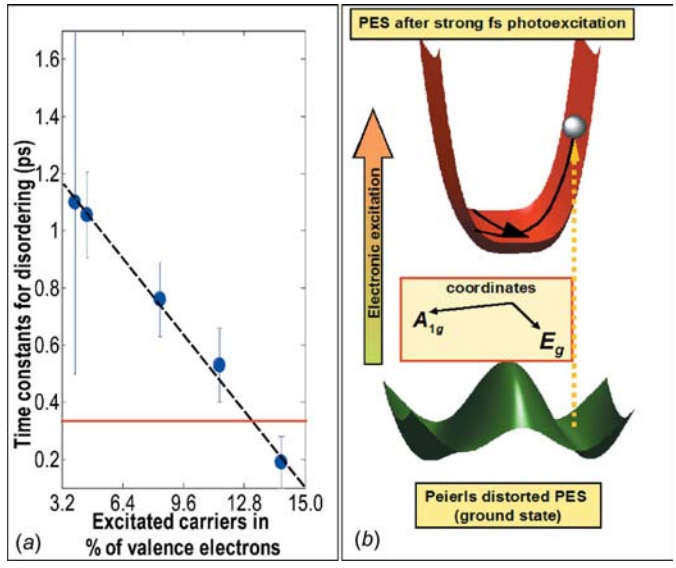

Figure 10
(*a*) Time constants for order to disorder, the process occurring in Bi as a function of the photoexcitaton level. The values were obtained from exponential fits of the $(1\bar{1}0)$ peak intensity decay. The dashed line was drawn as a guide to reflect the absence of a plateau. The red line denotes the period of the A_{1g} phonon in the ground state. (*b*) Illustrative changes in the PES after strong fs electronic excitation. The Peierls barrier disappeared and Bi atoms experience a large repulsive force that leads to very fast disordering. A strong anharmonic coupling between the longitudinal (A_{1g}) and transverse mode (E_g) is expected as well as the evolution of a saddle point. For more details see Sciaini *et al.* (2009).

these experiments, the film is permanently damaged after each laser shot (for sample preparation see Kammler & Horn-von Hoegen, 2005 and Payer *et al.*, 2008). These particular studies were conducted by averaging as few as ten single-shot diffraction patterns for different time delays. For cost reasons, a lens-coupled CCD detector with only 10% quantum efficiency was used for these studies. These measurements illustrate that the electron number density is sufficient for single-shot structure determinations with every-electron detectors such as standard fiber-coupled CCDs.

Fig. 10(*a*) shows the time constants for the disordering process occurring in strongly photoexcited Bi. As can be observed, the rate for the order-to-disorder process is strongly dependent on the excitation level and up to the limit that it is surprisingly faster than a period of the A_{1g} phonon mode (Cavalleri, 2009). The pronounced trend (dashed line in Fig. 10*a*) without evidence of slowing down and the timescales for the disordering process mirror the electronic–nonthermal nature of the driven force. The mechanism by which a crystalline distorted system reaches an isotropic liquid state on such extremely fast timescales was explained by a drastic change in the PES upon photoexcitation (Sciaini *et al.*, 2009). Fig. 10(*b*) illustrates the change in the PES after fs electronic excitation. The atoms, initially at the equilibrium position of the ground state, are strongly accelerated in a downhill pathway to anharmonically couple to an unstable transverse mode which brings the necessary shear motion to reach an isotropic liquid phase in a ballistic way.

This is the first example of ballistic melting. The observed timescales being less than a collision (as defined by the half period of the A_{1g} mode) and the linear dependence on the excitation dynamics illustrate that this is a driven process. As an analogy, these observations are akin to the accelerator on a car. Increasing the laser excitation is like pressing down on the pedal making the atoms go faster and faster. The observed timescale for this full-scale structural change is extraordinary. For calibration, the fastest chemical reaction known that involves nuclear motion is the *cis*- to *trans*- photoisomerization of the retinal chromophore in rhodopsin. This is a highly optimized reaction coordinate and corresponds to similar concepts of approaching a half period motion of the torsional motion (transverse-like motion) around the double bond. The torsional mode is referred to as the reaction mode. The heavy-atom motions involved in this reaction are only on the order of 0.1 Å. The PES of the protein is highly optimized to direct this process. In the case of Bi, bonds must break and the motions exceed 0.1 Å to sample sufficient nuclear configuration space to correspond to the liquid state. These motions are occurring faster than even photoisomerization of rhodopsin. This is a very strongly driven process at the highest excitation levels and it corresponds to the fastest structural transition observed to date.

The question is how fast could this process be made? At the moment the fs pulse is absorbed, the atoms have initial trajectories defined by their thermal population at room temperature. These random motions map onto the photo-induced changes in the potential energy landscape of the lattice in which there are repulsive gradients along the A_{1g} mode, anharmonic terms mixing the A_{1g} and E_g modes and reduction in barriers to transverse motions to interstitial regions. If one considers the instantaneous velocity of the atoms moving within the initial, approximately harmonic motion of the A_{1g} mode, this process could be considered to be going at approximately the mean speed of sound or Mach 1. Could it be driven even faster and redefine the limits to nuclear motions involved in structural rearrangements? We were unable to characterize the motions at higher excitation to find this fundamental limit for Bi (before plasma formation) as the time resolution was insufficient. Next-generation electron and X-ray sources will be able to resolve this issue.

Finally, in terms of picturing the overall mechanism, consider the initial electron distribution. The electron distribution follows the one-dimensional Peierls distortion of the lattice. It is the increased orbital overlap and electron density at these alternating pairs of Bi atoms that give rise to the Peierls stability. At high excitations, the electronic states are more diffuse, depleting electron density between the Bi dimers; there would be strong electron–electron correlation effects leading to a more spatially isotropic charge distribution. It is this change in electronic distribution that modifies the lattice potential. The atoms are driven to the isotropic liquid structure ballistically through this many-body electron–lattice coupling. It is a beautiful example of a many-body effect in both the electronic and nuclear coordinates.

3.6. Direct observation of collective modes: first step to proteins

This section follows up on the study of free-standing nm-thick single-crystalline Si membranes but under low excitation conditions. Single crystals make a significant difference in SNR over polycrystalline samples as the signal amplitude is localized in a single spot, giving amplification above diffuse background scatter. It is also possible to Fourier filter out the diffuse scatter. The challenge is obtaining high-quality, large-area, single crystals of the correct thickness. This work exploited the recent advances in fabricating sheets of Si using sacrificial etching of the buried oxide layer of a silicon-on-insulator structure (Roberts *et al.*, 2006; Scott & Lagally, 2007). It is possible to obtain single crystals of Si that have 10–100 nm thicknesses and surface areas of 25 mm^2. These crystals, which are so thin they can be bent but are still very strong, are now being touted as the template for high-speed 'plastic electronics'.

The experimental FED result for low photocarrier injection into Si (001) is shown in Fig. 11.

The collective modes excited by uniform relaxation of the photocarriers into heat (statistical relaxation into acoustic phonons) are clearly observable by eye. The surprise here is that one sees both the longitudinal and transverse acoustic modes. It is usually not possible to excite or detect transverse acoustic modes by optical excitation. The planar profile of the excitation couples selectively to longitudinal acoustic modes. Only in the case of an extremely tight focus, on the order of a

micron, is it possible to have significant strain fields in the transverse direction to observe the acoustics with comparable amplitude to longitudinal phonons (Rossignol *et al.*, 2005). This observation by itself is important as the full characterization of the mechanical properties of materials requires the speed of sound/elasticity measurements in both the longitudinal and transverse directions. Contact methods are normally required. The big virtue of optical excitation of sound fields is that it provides a contactless method of characterizing materials but until now could not provide information on the full elasticity tensor. With FED, we can now fully characterize the mechanical properties of nanoscale objects.

The new observation of transverse acoustic modes is due to the fact that electron diffraction is much more sensitive to transverse displacements than optical measurements. The diffraction process is most sensitive to motions transverse to the surface normal. There was an earlier study of acoustic phonons in Al where only the longitudinal modulation was observed (Nie *et al.*, 2006) for polycrystalline samples. It was difficult to understand this earlier work as one should not observe motion along the surface normal in electron diffraction. From the above work on Si (Harb *et al.*, 2009), we showed that the observation of coherent acoustic phonons arises from the coupling of the longitudinal and transverse modes through the surface deformation from nonuniform excitation and the intrinsically higher sensitivity of electron diffraction to transverse atomic motions.

Apart from providing a new approach to characterizing nanoscale objects, these results illustrate the high sensitivity of electron diffraction to the displacement of collective modes. From the change in the spot positions, the r.m.s. motions of the atomic displacements in phase with the acoustic mode are on the order of 10^{-3} Å. This amplitude is more than one order of magnitude smaller than the displacement of collective modes involved in the protein relaxation process and functionally relevant motions. FED has the potential to become a very powerful probe of strongly correlated motions in biological systems.

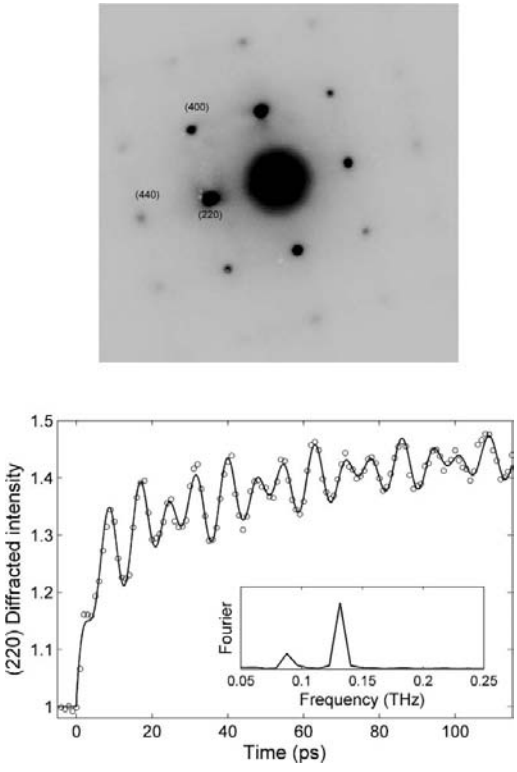

Figure 11
Direct observation of collective modes. The top panel shows the observed diffraction pattern and assignment of some key orders. The bottom panel shows the time-resolved changes in the intensity of the (220) diffraction order following photocarrier injection with low-intensity fs 400 nm pulses. The photocarriers relax *via* optical phonons ultimately into acoustic phonons. This thermalized energy leads to lattice expansion along the surface normal. Since the spatially Gaussian excitation pulses are nonuniform in the plane, there is also a surface deformation. The longitudinal expansion and surface deformation couple to excite longitudinal and transverse acoustic modes of the 33 nm-thick membrane that then oscillates. The Fourier transform of the oscillations is shown in the inset and corresponds exactly to the lowest-frequency longitudinal and transverse modes normal to the crystal (33 nm boundary condition on the half wavelength).

4. Perspective

4.1. Remaining challenges, pitfalls and the future

So far, the limitations of high-brightness electron sources for FED studies, in the enterprise of making molecular movies, have not been discussed. The biggest problem by far, for all electron-based probes, is the samples. There has been a long history of dealing with this problem in the field of electron microscopy. For transmission studies, the samples must be made between 10 and 100 nm thick. The samples generally need to be made thin enough to be in the single electron scattering event limit to avoid secondary or multiple electron scattering which may distort the diffraction process and lead to errors in structure determination in the inversion process. There are standard approaches to making samples of this thickness. However, the real challenge is to make large-area samples as required for movie-mode data acquisition. In this regard, the advent of nanotechnology and associated methods of nanofabrication will be invaluable. We have only begun to tap into this methodology in sample preparation. Our work in using Si nanofabrication methods to make sample support grids with each frame representing a time point or movie frame is one example. The other approach to solving this problem is to go to higher-energy electrons. We are now online with 100 keV machines and soon there will be 300 keV machines. The next generation of machines, with factors of 100 more electrons, ten times higher detection efficiency with 'every-electron detectors', and factors of 10 shorter pulses using RF pulse-compression cavities, will give an overall gain in effective brightness of 10^4 in recording time-dependent diffraction patterns over the results presented above.

Every method has its pitfalls and artifacts and electron diffraction is no exception. At the high excitations required to observe nonreversible structure changes, the short excitation pulses will lead to resonant multi-photon ionization of the

sample. Lattice charging from the excitation, not the electrons, will be limiting in many cases. The charging of insulating materials from the electron beam is also a standard problem and is normally solved using conductive carbon-coated grids to help discharge the sample. The photoinduced charging is more difficult to control as it is an intrinsic effect. For metals, the surface charge is localized at the surface to within 1 nm. In transmission, this effect is small relative to the overall sample thickness and the surface fields cancel out for propagation normal to the surface. This, however, is not the case for surface-sensitive probes such as ultrafast electron diffraction conducted in reflection mode. Recent studies show that this leads to artifacts and erroneous conclusions of fast structural dynamics that are actually related to the development of space-charge fields with the motion of the electrons away from the surface and not lattice dynamics (Park & Zuo, 2009). A number of studies attributing unusual effects involving correlated atomic motions normal to the surface using electron diffraction in reflection are most likely artifacts (see Park & Zuo, 2009 for a discussion on this point). In addition, the lattice-charging effects can also lead to structural changes at the surface that have nothing to do with excited lattice electrons but rather the photoemitted electrons. Structural changes in anisotropic crystals involving motion solely along the surface normal are probably from this source and need to be checked. Similarly, there are surface deformations and trivial thermal effects that must be distinguished from the photoinduced dynamics of interest. Control experiments are needed to assess these different signal contributions.

The above-cited problems have clearly been solved for the most part. The above studies have illustrated that the technology for directly observing atomic motions on the fs timescale has been achieved. The camera for the molecular movie is now in hand. The first applications of this newly developed methodology have been to study the simplest order-to-disorder transitions albeit with fs time resolution. We have been able to distinguish thermally propagated structural phase transitions from electronically driven structure changes. Through these studies we have determined the mechanisms involve nucleation sites on the nm, or molecular, scale. The notion of something undergoing homogeneous nucleation is even more intriguing when viewed at this atomic scale of inspection. In the case of electronically driven structural changes, the most important generalization is that directional bonding within the nascent material is needed in order for the optically induced changes in electron density to create gradients/forces for the displacement. In the case of Si, we have observed diffusive sampling of what can be considered electronically induced nucleation. The observations of Bi really capture the imagination. We have observed a ballistically driven phase transition that involves a many-body effect to evade the requirements of multiple collisions to sufficiently sample the nuclear configuration space for liquid formation. The changes in electronic density provide the forces that map the system onto the disordered liquid potential energy landscape. This work in particular has clearly demonstrated that it is possible to optically modify the potential energy landscape of materials. As the time resolution and brightness of next-generation technology improves, it will be interesting to see how far this concept can be pushed. The prospect of optically modifying the fundamental forces between atoms reached the ultimate limit with the creation of warm dense matter in which bond stiffening was observed for Au (before it became an unbound plasma). Higher excitation conditions and time resolution will undoubtedly lead to much needed new information for understanding the extreme physics of materials under high pressure and temperature, with laser-driven nuclear fusion as one potentially important application.

With respect to optically manipulating interatomic forces, we fully expect that coherent control protocols will soon be used in conjunction with structurally sensitive X-ray and electron probes. This will be an extension of the basic methodology now demonstrated with Bi. By explicitly exploiting phase in the optically prepared wavefunctions, on timescales faster than decoherence, it is possible to control chemical reactions and direct atoms along preferred paths. The current method of observing coherent control of matter is based on optical methods and, as discussed above, does not have sufficient information to unambiguously invert the control pulse shape to the actually induced atomic motions. With FED probes, it will be possible to directly observe the laser–matter interaction and induced coherent steering of matter waves.

In terms of the future, we again emphasize the importance of sample preparation. There are literally thousands of problems that could be solved through an atomic level inspection of the structural dynamics. Whether one uses electrons or X-rays to study the structural dynamics, it will be nontrivial to fabricate the samples. Clever new ways of exploiting nanofabrication and handling of nanoscale materials will be needed to bridge the gap from making the molecular movie film to shooting the movie. The most general solution to this problem will be to use samples that can be easily replenished between laser shots, *i.e.* the simplest solution is to use gas-phase and liquid-phase samples with flow. Because of the extremely small scattering cross section for X-rays, electrons will be the preferred probe for gas-phase studies; whereas X-rays are the best probe for solution-phase studies. In this respect, it is clear that the recent advances in ultrabright electron-source technology and X-ray source technology will provide complementary approaches to atomically resolved structural dynamics.

4.2. The grand challenge: the structure–function correlation in biology

As emphasized in §1.3.2, the transition state is the unifying concept connecting chemistry and biology. This grand thought experiment has now become subject to direct experimental observation. The simple example given above with respect to the well defined static differences in structure in the binding of oxygen to hemoglobin was to illustrate that our understanding of what physically constitutes a critical point or transition-state region in a reaction coordinate is poorly developed for complex molecules. As with all scientific endeavors, the finer

the resolution of an observation the better our understanding of the phenomenon of interest becomes. So far, we have only very coarse views of transition-state processes. The acuity of our vision has now improved dramatically. We now have the necessary spatio-temporal resolution to watch chemistry as it happens. This new field of atomically resolved structural dynamics has the potential to revolutionize our understanding of chemistry. After all, we are approaching the fundamental limit in time and space by which we can observe chemical processes. In doing so, we will better appreciate what forces are at play in the barrier-crossing region and better design synthetic means to control barrier crossings once this connection is made.

By directly observing atomic motions during a biological function, we will arrive at a direct determination of the structure–function correlation. The collective mode coupling model discussed above will be uniquely tested and the key modes coupled to reaction coordinates will be revealed. It will only be possible to study a few model systems, at least initially. These systems include heme proteins, photoactive receptors and energy storage systems such as the family of rhodopsins and light-harvesting systems. This relatively small group will provide structural details for a certain subgroup of topological features from which it should be possible to generalize. Of course, obtaining sufficient numbers of crystals to conduct such studies is a challenge. However, the brightness of the next-generation electron and X-ray sources is high enough to bring this aspect of the problem to a manageable level. The problem is important enough that the sample limitations will be solved.

We are now at a turning point in science where we can literally send probes into the transition-state region to beam back pictures of what the energy landscape looks like. The above studies indicate that we can also optically manipulate these potential energy landscapes. This level of information will allow us to take complex multidimensional processes and convert them to a reduced reaction landscape, projecting out the key modes coupled to reaction coordinates. At this point, we will be able to rival Mother Nature in the control of chemical processes.

This work was supported by the Natural Sciences and Engineering Research Council of Canada, the Canada Foundation for Innovation and the Ontario Centres of Excellence. RE thanks the Alexander von Humboldt Foundation for financial support.

References

Abe, M., Ohtsuki, Y., Fujimura, Y. & Domcke, W. (2005). *J. Chem. Phys.* **123**, 144508.
Adelman, S. A. (1987). *Rev. Chem. Intermediates*, **8**, 321–338.
Armstrong, M. R., Ogilvie, J. P., Cowan, M. L., Nagy, A. M. & Miller, R. J. D. (2003). *Proc. Natl Acad. Sci. USA*, **100**, 4990–4994.
Behnia, K., Balicas, L. & Kopelevich, Y. (2007). *Science*, **317**, 1729–1731.
Bernstein, R. B. (1982). *Chemical Dynamics by Molecular Beam and Laser Techniques*. Oxford University Press.
Biswas, R. & Ambegaokar, V. (1982). *Phys. Rev. B*, **26**, 1980–1988.
Born, M. (1939). *J. Chem. Phys.* **7**, 591–603.
Bottin, F. & Zerah, G. (2007). *Phys. Rev. B*, **75**, 174114.
Bucksbaum, P. H., Schumacher, D. W. & Bashkansky, M. (1988). *Phys. Rev. Lett.* **61**, 1182–1185.
Cammarata, M., Levantino, M., Schotte, F., Anfinrud, P. A., Ewald, F., Choi, J., Cupane, A., Wulff, M. & Ihee, H. (2008). *Nature Meth.* **5**, 881–886.
Carbone, F., Yang, D.-S., Giannini, E. & Zewail, A. H. (2008). *Proc. Natl Acad. Sci. USA*, **105**, 20161–20166.
Cavalleri, A. (2009). *Nature* (*London*), **458**, 42–43.
Cavalleri, A., Siders, C. W., Rose-Petruck, C., Jimenez, R., Toth, C., Squier, J. A., Barty, C. P. J., Wilson, K. R., Sokolowski-Tinten, K., von Hoegen, M. H. & von der Linde, D. (2001). *Phys. Rev. B*, **63**, 193306.
Collet, E., Lemée-Cailleau, M.-H., Buron-Le Cointe, M., Cailleau, H., Wulff, M., Luty, T., Koshihara, S.-Y., Meyer, M., Toupet, L., Rabiller, P. & Techert, S. (2003). *Science*, **300**, 612–615.
Coppens, P. (2003). *Chem. Commun.* **9**, 1317–1320.
Corkum, P. B. & Chang, Z. (2008). *Opt. Photon. News*, **19**, 24–29.
Dudek, R. C. & Weber, P. M. (2001). *J. Phys. Chem. A*, **105**, 4167–4171.
Dumitrica, T., Burzo, A., Dou, Y. & Allen, R. E. (2003). *Fifth Motorola Workshop on Computational Materials and Electronics*, pp. 2331–2342. Austin, TX, USA.
Dwyer, J. R., Hebeisen, C. T., Ernstorfer, R., Harb, M., Deyirmenjian, V. B., Jordan, R. E. & Miller, R. J. D. (2006). *Philos. Trans. R. Soc. A*, **364**, 741–778.
Ernstorfer, R., Harb, M., Hebeisen, C. T., Sciaini, G., Dartigalongue, T. & Miller, R. J. D. (2009). *Science*, **323**, 1033–1037.
Evans, M. G. & Polanyi, M. (1935). *Trans. Faraday Soc.* **31**, 0875–0893.
Eyring, H. (1935). *J. Chem. Phys.* **3**, 107–115.
Fritz, D. M. *et al.* (2007). *Science*, **315**, 633–636.
Geer, S. B. van der, Luiten, O. J. & de Loos, M. J. (2007). *Int. J. Mod. Phys. A*, **22**, 4000–4005.
Goodno, G. D. & Miller, R. J. D. (1999). *J. Phys. Chem. A*, **103**, 10619–10629.
Guo, C., Rodriguez, G., Lobad, A. & Taylor, A. J. (2000). *Phys. Rev. Lett.* **84**, 4493–4496.
Harb, M. (2009). PhD thesis, University of Toronto, Canada.
Harb, M., Ernstorfer, R., Dartigalongue, T., Hebeisen, C. T., Jordan, R. E. & Miller, R. J. D. (2006). *J. Phys. Chem. B*, **110**, 25308–25313.
Harb, M., Ernstorfer, R., Hebeisen, C. T., Sciaini, G., Peng, W., Dartigalongue, T., Eriksson, M. A., Lagally, M. G., Kruglik, S. G. & Miller, R. J. D. (2008). *Phys. Rev. Lett.* **100**, 155504.
Harb, M., Peng, W., Sciaini, G., Hebeisen, C. T., Ernstorfer, R., Eriksson, M. A., Lagally, M. G., Kruglik, S. G. & Miller, R. J. D. (2009). *Phys. Rev. B*, **79**, 094301.
Hastings, J. B., Rudakov, F. M., Dowell, D. H., Schmerge, J. F., Cardoza, J. D., Castro, J. M., Gierman, S. M., Loos, H. & Weber, P. M. (2006). *Appl. Phys. Lett.* **89**, 184109.
Hebeisen, C. T. (2009). PhD thesis, University of Toronto, Canada.
Hebeisen, C. T., Ernstorfer, R., Harb, M., Dartigalongue, T., Jordan, R. E. & Miller, R. J. D. (2006). *Opt. Lett.* **31**, 3517–3519.
Hebeisen, C. T., Sciaini, G., Harb, M., Ernstorfer, R., Dartigalongue, T., Kruglik, S. G. & Miller, R. J. D. (2008). *Opt. Express*, **16**, 3334–3341.
Hebeisen, C. T., Sciaini, G., Harb, M., Ernstorfer, R., Kruglik, S. G. & Miller, R. J. D. (2008). *Phys. Rev. B*, **78**, 081403.
Huang, W. J., Zuo, J. M., Jiang, B., Kwon, K. W. & Shim, M. (2009). *Nature Phys.* **5**, 129–133.
Johnson, S. L., Beaud, P., Vorobeva, E., Milne, C. J., Murray, É. D., Fahy, S. & Ingold, G. (2009). *Phys. Rev. Lett.* **102**, 175503.
Kammler, M. & Horn-von Hoegen, M. (2005). *Surf. Sci.* **576**, 56–60.
Kandyla, M., Shih, T. & Mazur, E. (2007). *Phys. Rev. B*, **75**, 214107.
Kapitza, P. L. & Dirac, P. A. M. (1933). *P. Camb. Philos. Soc.* **29**, 297–300.

Kibble, T. W. B. (1966). *Phys. Rev. Lett.* **16**, 1054–1056.
Kim, T. K., Lee, J. H., Wulff, M., Kong, Q. & Ihee, H. (2009). *ChemPhysChem*, **10**, 1958–1980.
King, W. E., Campbell, G. H., Frank, A., Reed, B., Schmerge, J. F., Siwick, B. J., Stuart, B. C. & Weber, P. M. (2005). *J. Appl. Phys.* **97**, 111101.
Kita, Y., Vanzytveld, J. B., Morita, Z. & Iida, T. (1994). *J. Phys. Condens. Matter*, **6**, 811–820.
Leu, B. M., Ching, T. H., Zhao, J., Stuhahn, W., Alp, E. E. & Sage, J. T. (2009). *J. Phys. Chem. B*, **113**, 2193–2200.
Lin, Z., Zhigilei, L. V. & Celli, V. (2008). *Phys. Rev. B*, **77**, 075133.
Lindenberg, A. M. *et al.* (2005). *Science*, **308**, 392–395.
Lorenc, M., Hébert, J., Moisan, N., Trzop, E., Servol, M., Buron-Le Cointe, M., Cailleau, H., Boillot, M. L., Pontecorvo, E., Wulff, M., Koshihara, S. & Collet, E. (2009). *Phys. Rev. Lett.* **103**, 028301.
Lundqvist, B. & Lundqvist, B. (1973). Editors. *Nobel Symposium 24; Collective Properties of Physical Systems*, pp. 84–120. New York: Academic Press.
Madelung, O., Rössler, U. & Schulz, M. (1998). Bismuth (Bi) crystal structure; chemical bond. In *Semiconductors*, Vol. 41, sub-vol. C: *Non-Tetrahedrally Bonded Elements and Binary Compounds I.* USA: Springer.
Miller, R. J. D. (2002). *Can. J. Chem.* **80**, 1–24.
Murray, E. D., Fritz, D. M., Wahlstrand, J. K., Fahy, S. & Reis, D. A. (2005). *Phys. Rev. B*, **72**, 060301.
Nagy, A., Prokhorenko, V. & Miller, R. J. D. (2006). *Curr. Opin. Struct. Biol.* **16**, 654–663.
Nie, S., Wang, X., Park, H., Clinite, R. & Cao, J. (2006). *Phys. Rev. Lett.* **96**, 025901.
Oudheusden, T. van, de Jong, E. F., van der Geer, S. B., Root, W., Luiten, O. J. & Siwick, B. J. (2007). *J. Appl. Phys.* **102**, 093501.
Park, H. & Zuo, J. M. (2009). *Appl. Phys. Lett.* **94**, 251103.
Payer, Th., Rajković, I., Ligges, M., Von Der Linde, D., Horn-Von Hoegen, M. & Meyer Zu Heringdorf, F.-J. (2008). *Appl. Phys. Lett.* **93**, 093102.
Peierls, R. E. (1991). *More Surprises in Theoretical Physics*, pp. 24–26. USA: Princeton University Press.
Perutz, M. F., Kilmartin, J. V., Nagai, K., Szabo, A. & Simon, S. R. (1976). *Biochemistry*, **15**, 378–387.
Pilling, M. J. & Seakins, P. W. (1995). *Reaction Kinetics*, 2nd ed. Oxford University Press.
Polanyi, J. C. & Zewail, A. H. (1995). *Acc. Chem. Res.* **28**, 119–132.
Recoules, V., Clerouin, J., Zerah, G., Anglade, P. M. & Mazevet, S. (2006). *Phys. Rev. Lett.* **96**, 055503.
Reed, B. W. (2006). *J. Appl. Phys.* **100**, 034916.
Rice, S. A. (1992). *Science*, **258**, 412–413.
Roberts, M., Klein, L. J., Savage, D. E., Slinker, K. A., Friesen, M., Celler, G., Eriksson, M. A. & Lagally, M. G. (2006). *Nature Mater.* **5**, 388–393.
Rossignol, C., Rampnoux, J. M., Perton, M., Audoin, B. & Dilhaire, S. (2005). *Phys. Rev. Lett.* **94**, 166106.
Rousse, A., Rischel, C., Fourmaux, S., Uschmann, I., Sebban, S., Grillon, G., Balcou, P., Foster, E., Geindre, J. P., Audebert, P., Gauthier, J. C. & Hulin, D. (2001). *Nature* (*London*), **410**, 65–68.
Schotte, F., Lim, M., Jackson, T. A., Smirnov, A. V., Soman, J., Olson, J. S., Phillips, G. N. Jr, Wulff, M. & Anfinrud, P. A. (2003). *Science*, **300**, 1944–1947.
Sciaini, G., Harb, M., Kruglik, S. G., Payer, Th., Hebeisen, C. T., Meyer zu Heringdorf, F.-J., Yamaguchi, M., Horn von Hoegen, M., Ernstorfer, R. & Miller, R. J. D. (2009). *Nature* (*London*), **458**, 56–59.
Scott, S. A. & Lagally, M. G. (2007). *J. Phys. D*, **40**, R75–R92.
Seidner, L. & Domcke, W. (1994). *Chem. Phys.* **186**, 27–40.
Seno, Y. J. & Go, N. (1990). *J. Mol. Biol.* **216**, 95–109.
Shank, C. V., Yen, R. & Hirlimann, C. (1983). *Phys. Rev. Lett.* **51**, 900–902.
Shapiro, M. & Brumer, P. (2003). *Principles of the Quantum Control of Molecular Processes.* New York: Wiley.
Siders, C. W., Cavalleri, A., Sokolowski-Tinten, K., Toth, C., Guo, T., Kammler, M., von Hoegen, M. H., Wilson, K. R., von der Linde, D. & Barty, C. P. J. (1999). *Science*, **286**, 1340–1342.
Siwick, B. J., Dwyer, J. R., Jordan, R. E. & Miller, R. J. D. (2002). *J. Appl. Phys.* **92**, 1643–1648.
Siwick, B. J., Dwyer, J. R., Jordan, R. E. & Miller, R. J. D. (2003). *Science*, **302**, 1382–1385.
Sokolowski-Tinten, K., Blome, C., Blums, J., Cavalleri, A., Dietrich, C., Tarasevitch, A., Uschmann, I., Förster, E., Kammler, M., Horn-von-Hoegen, M. & von der Linde, D. (2003). *Nature* (*London*), **422**, 287–289.
Srajer, V., Ren, Z., Teng, T. Y., Schmidt, M., Ursby, T., Bourgeois, D., Pradervand, C., Schildkamp, W., Wulff, M. & Moffat, K. (2001). *Biochemistry*, **40**, 13802–13815.
Stampfli, P. & Bennemann, K. H. (1994). *Phys. Rev. B*, **49**, 7299–7305.
Techert, S., Schotte, F. & Wulff, M. (2001). *Phys. Rev. Lett.* **86**, 2030–2033.
Voth, G. A. & Hochstrasser, R. M. (1996). *J. Phys. Chem.* **100**, 13034–13049.
Walther, M., Raicu, V., Ogilvie, J. P., Phillips, R., Kluger, R. & Miller, R. J. D. (2005). *J. Phys. Chem. B*, **109**, 20605–20611.
Weinacht, T. C., White, J. L. & Bucksbaum, P. H. (1999). *J. Phys. Chem. A*, **103**, 10166–10168.
Williamson, J. C., Dantus, M., Kim, S. B. & Zewail, A. H. (1992). *Chem. Phys. Lett.* **196**, 529–534.
Williamson, S. & Mourou, G. (1984). *Phys. Rev. Lett.* **52**, 2364–2367.
Yang, F. Y., Liu, K., Hong, K., Reich, D. H., Searson, P. C. & Chien, C. L. (1999). *Science*, **284**, 1335–1337.
Zhang, J. & Zuo, J. M. (2009). *Carbon*, **47**, 3515–3528.
Zhang, Y., Fujisaki, H. & Straub, J. E. (2009). *J. Chem. Phys.* **130**, 025102.
Zijlstra, E. S., Tatarinova, L. L. & Garcia, M. E. (2006*a*). *Phys. Rev. B*, **74**, 220301.
Zijlstra, E. S., Tatarinova, L. L. & Garcia, M. E. (2006*b*). *Proc. SPIE*, **6261**, 62610R.
Zijlstra, E. S., Walkenhorst, J. & Garcia, M. E. (2008). *Phys. Rev. Lett.* **101**, 135701.